Volume 15
Number 2

December *2013*
(ISSN 1109-1606)

Journal of APPLIED ELECTROMAGNETISM

JAE

Institute of Communication and Computer Systems

Athens - GREECE

Volume 15 December 2013
Number 2 (ISSN 1109-1606)

JOURNAL
OF
APPLIED ELECTROMAGNETISM

Trans Black Sea Region Union of Applied Electromagnetism

BSUAE

Institute of Communication and Computer Systems

Athens - GREECE

Volume 15 **Number 2**

December 2013

TRANS BLACK SEA REGION UNION OF APPLIED ELECTROMAGNETISM (BSUAE)

JOURNAL OF APPLIED ELECTROMAGNETISM

Institute of Communication and Computer Systems

Athens - GREECE

Editor: Panayiotis Frangos (Greece), pfrangos@central.ntua.gr

Honorary Editor: Nikolaos K. Uzunoglu (Greece), nuzu@central.ntua.gr

Board of Associate Editors

D. Dimitrov (Bulgaria), dcd@tu-sofia.bg
V. Dumbrava (Lithuania), vydum@ktu.lt
G. Georgiev (Bulgaria), gngeorgiev@yahoo.com
G. Matsopoulos (Greece), gmatso@esd.ece.ntua.gr

Editorial Board

ALBANIA
G. Bardhyf, bardhylgolemi@live.com
C. Pirro, p_cipo@yahoo.com

ARMENIA
H. Bagdasarian, hovik@seua.sci.am
H. Terzian, hterzian@seua.sci.am

BULGARIA
A. Antonov, asantonov@abv.bg
A. Lazarov, lazarov@bfu.bg
S. Savov, savovsv@yahoo.com

GEORGIA
R. Zaridze, rzaridze@laetsu.org

GERMANY
M. Georgieva – Grosse, mngeorgieva@yahoo.de

GREECE
H. Anastassiu, ANASTASIOU.Christos@haicorp.com
I. Avramopoulos, hav@mail.ntua.gr
G. Fikioris, gfiki@cc.ece.ntua.gr
J. Kanellopoulos, ikanell@cc.ece.ntua.gr
G. Karagiannidis, geokarag@auth.gr
G. Kliros, gsksma@hol.gr
T. Mathiopoulos, mathio@space.noa.gr
C. Moschovitis, harism@noc.ntua.gr
K. Nikita, knikita@cc.ece.ntua.gr
I. Ouranos, iouranos@central.ntua.gr
E. Papkelis, spapkel@central.ntua.gr
J. Sahalos, sahalos@auth.gr
M. Theologou, theolog@cs.ntua.gr

N. Triantafyllou, nitriant@central.ntua.gr
K. Ksystra, katksy@central.ntua.gr
A. Malamou, annamalamou@yahoo.gr

JORDAN
N. Dib, nihad@just.edu.jo

KAZAKSHTAN
S. Sautbekov, sautbek@mail.ru

LITHUANIA
L. Svilainis, linas.svilainis@ktu.lt

RUSSIA
M. Bakunov, bakunov@rf.unn.runnet.ru
A. Grigoriev, adgrigoriev@mail.ru

SERBIA
B. Reljin, ereljin@ubbg.etf.bg.ac.yu

SPAIN
E. Gago – Ribas, egr@tsc.uniovi.es
M. Gonzalez – Morales, gonmor@yllera.tel.uva.es

UNITED KINGDOM
G. Goussetis, G.Goussetis@hw.ac.uk

Publishing Department

M. Georgieva – Grosse, mngeorgieva @yahoo.de
N. Triantafyllou, nitriant@central.ntua.gr
K. Ksystra, katksy@central.ntua.gr
A. Malamou, annamalamou@yahoo.gr

Journal of Applied Electromagnetism

Copyright Form

The undersigned I confirm that I agree the publication of the article

in the Journal of Applied Electromagnetism and the copyright to belong to Trans Black Sea Union of Applied Electromagnetism. I understand that I have the full right to reuse this manuscript for my own purposes.

Name:

Surname:

Address:

E-mail:

Signed:

***Please send the previous form signed either by e-mail to pfrangos@central.ntua.gr , or by fax to the fax number: +30 210 772 2281, attention of Prof. P. Frangos.**

Address

Institute of Communication and Computer Systems

National Technical University of Athens

9, Iroon Polytechniou str.

15773 Athens - GREECE

Tel: (+30) 2107723694

Fax: (+30) 2107722281, attention of Prof. P. Frangos

e-mail: pfrangos@central.ntua.gr

Web site: **http://jae.ece.ntua.gr**

TRANS BLACK SEA REGION UNION OF APPLIED ELECTROMAGNETISM (BSUAE)

JOURNAL OF APPLIED ELECTROMAGNETISM (JAE)

Volume 15 Number 2 December 2013

CONTENTS

NETWORK PLANNING AND QOS SIMULATION SOFTWARE DESIGN FOR 4TH GENERATION BROADBAND WIRELESS TECHNOLOGIES

L. Narbutaitė, R. Brūzgienė, E. Kačerginskis 1

Mobile network design is complex task that requires evaluation of many parameters that allow service providers to plan optimal network coverage and select mobility management solutions. It's especially relevant for such new technologies as LTE or mobile WiMAX, where ability to simulate network behavior is very important before starting real network implementation. This article presents software that was designed for 4th generation broadband wireless network planning, QoS simulation and analysis. Software consists of three major modules that allow estimating wireless propagation for different modulation techniques, simulating wireless protocols, estimating base station distribution and calculating cumulated data traffic in different types of overlapping wireless sectors. Article analyzes software functionality, operation algorithms, demonstrates possible network planning and simulation scenarios.

THE DOUBLE AND TRIPLE RESONANCES INVESTIGATION FOR THE "CASSINI" LATTICE INTO THE DIELECTRIC

I. M. Petoev, V. A. Tabatadze, R. S. Zaridze 8

The double and triple resonance effects for the certain metal – dielectric structure are studied. The structure represents the three dimensional periodic "Cassini" lattice inside of the usual dielectric with the finite sizes. The lattice element is a conductor wire with small electrical radius and with the form of the Cassini oval. Such structures have the interesting resonance properties in the wide frequency range, which makes it possible to present them as the complex materials. The program package was created and it gives the ability to study resonance properties of these structures. In the developed program package it is possible to change the parameters of the studied structure making advantage of numerical experiments.

EXPERIMENTAL STUDY OF THE INFLUENCE OF AEROSOL PARTICLES ON LINK RANGE OF FREE SPACE LASER COMMUNICATION SYSTEM IN IRAQ

J. M. Jassim , A. K. Kodeary **28**

Attenuation due to aerosols restricts the distance of FSO communication systems and limits the availability for line-of-sight terrestrial link. This work is focused on the effect of aerosols on the FSO link. The attenuations was studied in the Hilla city in the aerosols phenomena for three selected wavelengths (532, 1064, and 10600 nm) for horizontal transmitting range (1-10) Km. The results show that system availability as a function of the range, and indicate that FSO systems can be deployed with reliability in Hilla city of Iraq.

METHODS AND ALGORITHMS FOR GENERATION OF RANDOM LOW FREQUENCY SERIES OF SIGNALS FOR MAGNETOTHERAPY

A. D. Dimitrov, K. L. Dimitrov **34**

Today most of the medical systems for magneto therapy contain digital control unit which provides more advanced features for treatment of different diseases. New systems for magneto therapy with pseudo-random frequency hopping provide more opportunities and better medical results.
The method described in this article shows new innovative way of generation of pseudo-random low frequency magnetic field. Due to the randomness character of device's output signals would be achieved reduced adaptation by human body to the influence of magnetic field and better treatment of different diseases.
However this algorithm is more complex it does not requires usage of any addi-tional elements and investment of high costs. The application of software methods for generation of pseudo-random signal frequency hopping in systems for magneto therapy can open new possibilities for treatment of more health diseases with better clinical results.

NETWORK PLANNING AND QOS SIMULATION SOFTWARE DESIGN FOR 4TH GENERATION BROADBAND WIRELESS TECHNOLOGIES

(Selected from CEMA'12 Conference)

L. Narbutaitė, R. Brūzgienė, E. Kačerginskis

Kaunas University of Technology, Department of Telecommunications
Studentų str. 50-452, Kaunas, Lithuania, LT-51368
lina.narbutaite@ktu.lt

Abstract

Mobile network design is complex task that requires evaluation of many parameters that allow service providers to plan optimal network coverage and select mobility management solutions. It's especially relevant for such new technologies as LTE or mobile WiMAX, where ability to simulate network behavior is very important before starting real network implementation. This article presents software that was designed for 4th generation broadband wireless network planning, QoS simulation and analysis. Software consists of three major modules that allow estimating wireless propagation for different modulation techniques, simulating wireless protocols, estimating base station distribution and calculating cumulated data traffic in different types of overlapping wireless sectors. Article analyzes software functionality, operation algorithms, demonstrates possible network planning and simulation scenarios.

1. INTRODUCTION

4Th generation broadband wireless technologies, such as mobile WiMAX and LTE are entering Telco markets, offering newest and most innovative technologies that allow to meet growing demand for mobility and data throughputs. The main goal is to achieve quality similar to wired technologies, enabling seamless use of VoIP, Video and data download services. Despite standards state very high efficiency of 4th generation technologies, it's not easy to achieve it real world environment.

One of the biggest challenges for service providers is to plan and implement such networks, because it requires evolution of many complex solutions, from network planning at the start to QoS modeling at the end. These tasks must be performed at the most possible detail manner in order to achieve best solution optimizing QoS, CAPEX and OPEX.

These major tasks must be performed by network implementation team:

- network equipment selection and base station coverage estimation, enabling services providers to decide what services are possible in certain areas and what equipment is requires to achieve desired data throughputs;

- simulation of wireless protocols that allows to evaluate performance of different services, select solutions for mobility management;
- network coverage planning, that allows to decide what are optimal distances between base stations, minimize zones with overlapping base station coverage and maximize network coverage without gaps and shadow zones;
- Handover overhead estimation, ensuring that designed network will be able to handle multiple users, especially in growing networks.

Automation of these tasks requires very expensive software usually provided by different vendors. It makes network implementation even more complex and time consuming project.

This article provides overview of Authors designed software package that allows service providers to ease network design and implementation tasks. Possible network planning and simulation scenarios are provided. Package consists of three software tools:

- base station (BS) coverage estimation software;
- protocol simulation software;
- network coverage estimation and handover overhead calculation software.

2. BS COVERAGE ESTIMATION

Base station coverage estimation software allows predicting radio signal attenuation in different line of sight and non-line of sight environments. It utilizes four mathematical models that can be used for coverage estimation in urban, suburban and rural areas: Direct line of sight, Walfish-Ikegami, Walfish-Ikegami geometrical and Stanford University Interim (SUI) models [1]. Software provides descriptions for each model and allows users to select or input required parameters.

Results are provided in graphical and text formats, showing estimated distance for different modulations used with OFDMA multiplexing technique (from QPSK to 64QAM). Higher rate modulations are more sensitive to propagation loss resulting shorter base station coverage radius. This must be taken into account when selecting what data throughput is required for planned services.

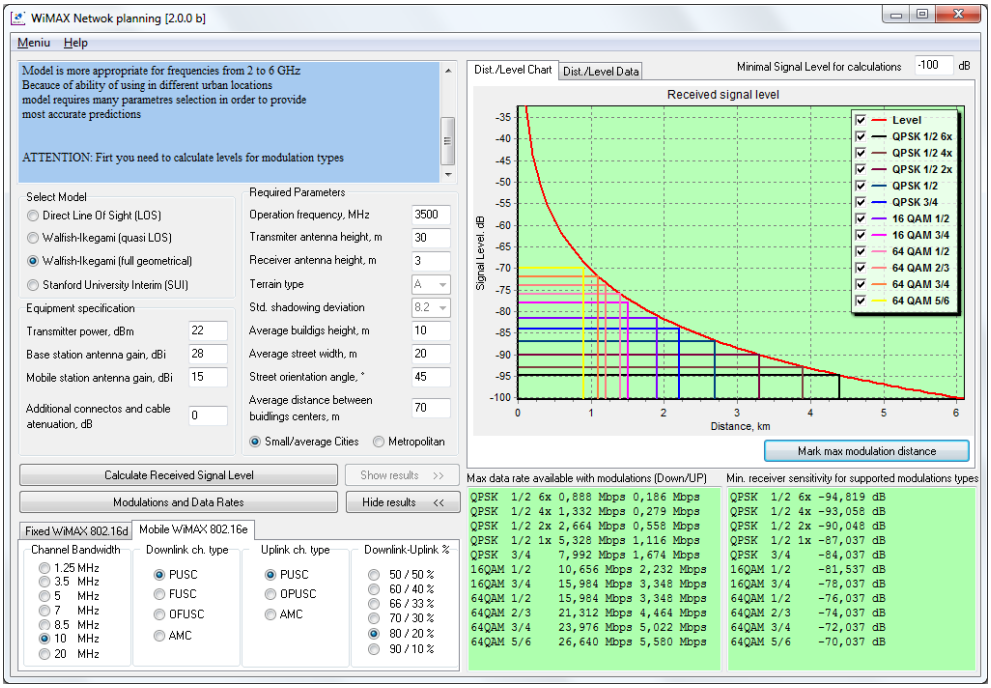

Figure 1. User interface of BS coverage estimation software

In addition to software provides fixed and mobile WiMAX data calculation plugin, which allows selecting channel bandwidth, subcarrier permutation schemes and calculating available data throughput for each modulation. Calculation examples are provided in Fig. 2, assuming in parameters provided in Table 1.

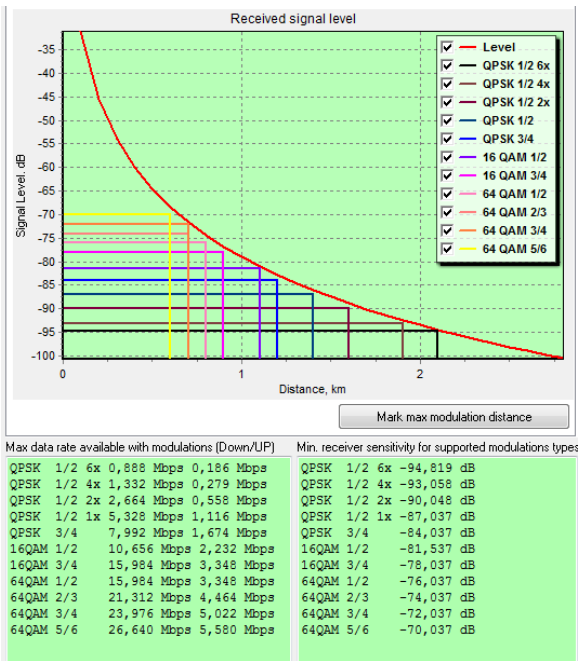

Figure 2. Distance and throughput estimation example

Table 1. Parameters used for calculation

Parameter	Value
Model	SUI-A (Urban environment)
Tx power	23 dBm
BS antenna gain	28 dBi
MS antenna gain	9 dBi
Frequency	3500 MHz
Channel size	10 MHz
Downlink/uplink ratio	80/20%

In this example case scenario we can see that radius of one base station can reach about 2 Km. Taking into account data throughput that is desired by service provider (for example 15 Mbps – 16QAM) it is required to plan base station coverage not higher than 1,4 Km.

3. SIMULATION OF PROTOCOLS

No spacing before and after paragraphs is needed. No footer or Header caption is recommended. Page numbering is obligatory.

Protocol simulation software is based on mathematical imitative simulation model which describes each network element as separate aggregate with input and output signals. Each aggregate and signal involves set of parameters and can represent behavior of mobile station, wireless channel, base station and connectivity network. Software user interface visualizes the mathematical model allowing users easily construct their network architecture and enter simulated protocol parameters such as channel latency, error probabilities, etc.

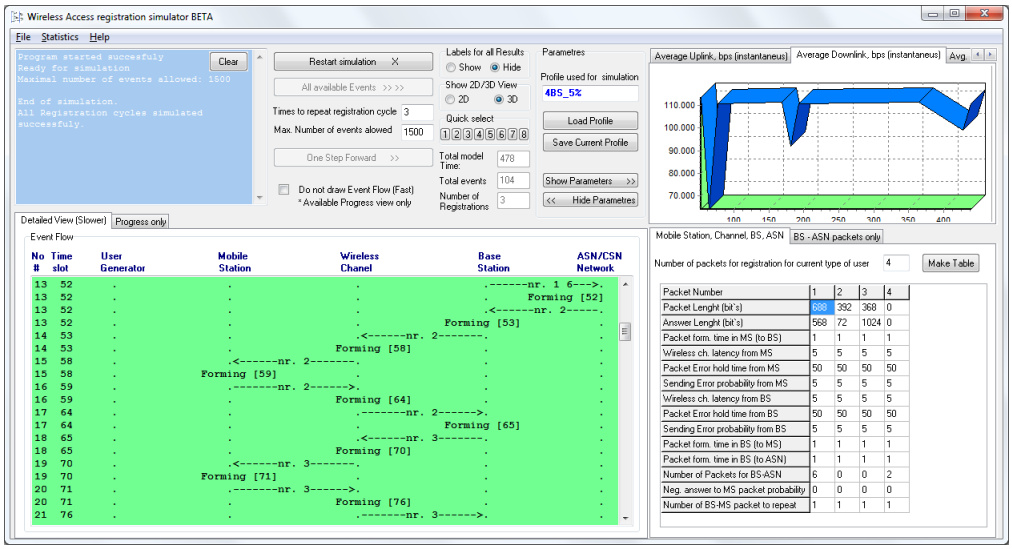

Figure 3. Simulation software GUI

Software allows creating, saving and restoring different simulation profiles for efficient comparison of investigated protocols. Simulation can be performed either step by step, analyzing each packet in time flow diagrams, either as complete simulation for thousands of simulated procedures. Software provides graphical results for different QoS characteristics of each network element – generated traffic, latency, average results, etc.

This article provides mobile WiMAX handover procedure simulation example. Procedure time flow diagram is provided in Fig. 4 [2].

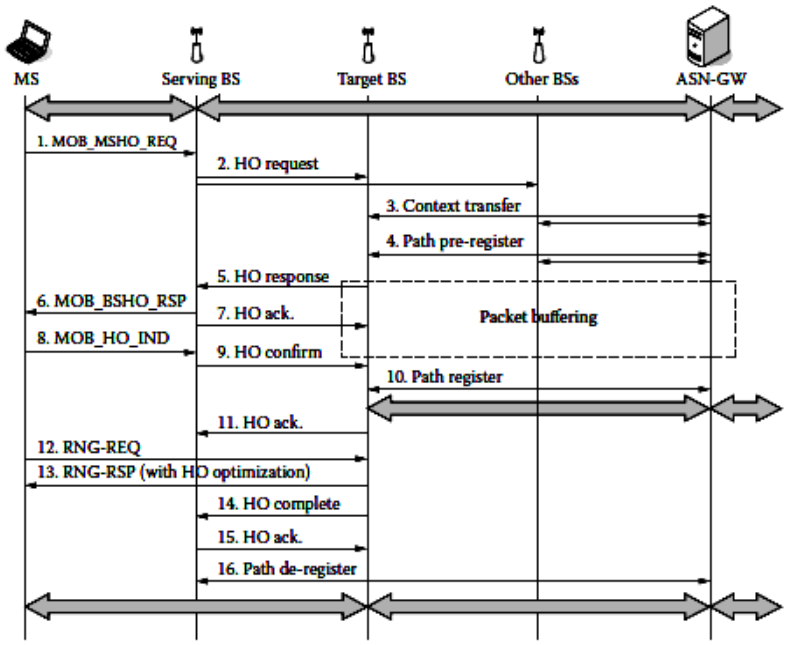

Figure 4. Handover time flow diagram

Diagram represents registration procedure and packets used for performing handover procedure. Describing each packet in simulation software was based on mobile WiMAX standard [1]. Simulation results are provided in Table 2. Values represent results when mobile station is in coverage from 2 to 4 base stations.

Table 2. mobile WiMAX handover simulation results

QoS Characteristics	Result
Handover latency	from 92 to 180 ms
Uplink generated data load	from 2.5 to 7 kbps
Downlink generated data load	from 3 to 9.5 kbps

As we can see registration procedure of one user is acceptable from latency point of view and does not create high data traffic, but when implementing network it must be taken into account, because network consists of many mobile stations and in overlapping network zones where could be continuous handover activity.

3. NETWORK COVERAGE EVALUATION

Network coverage evaluation software utilizes results of BS coverage estimation and protocol simulation. Software suggests optimal distance between base stations, provides graphical representation of base station coverage and calculates areas between all types of overlapping sectors. It allows specifying number of mobile stations in each area type and inputting traffic load.

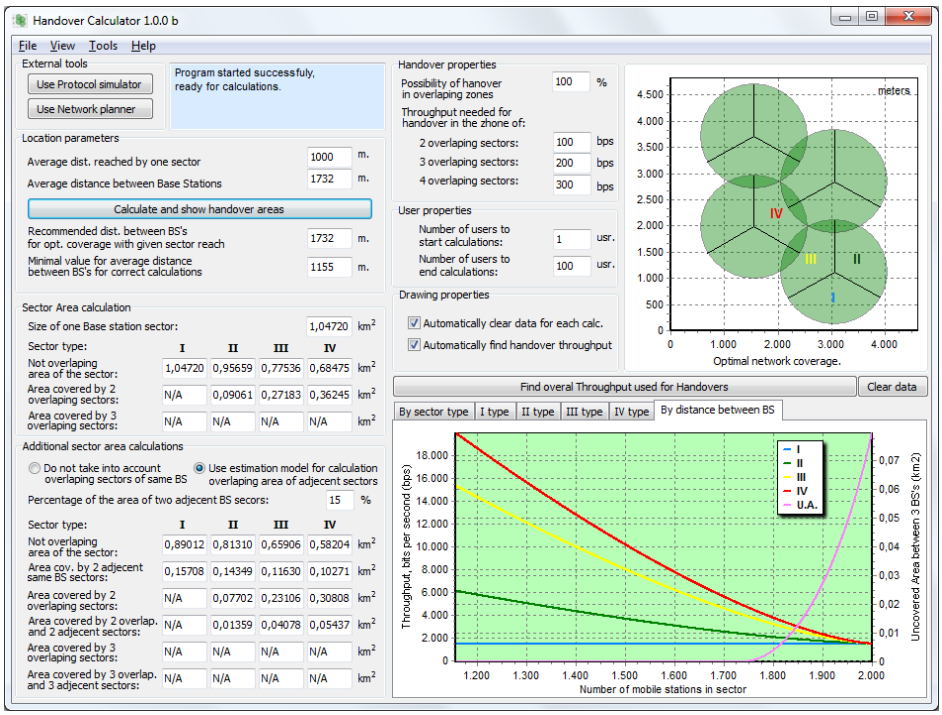

Figure 5. Network coverage evaluation software GUI

Calculation examples are provided in Figure 6, assuming that there are 25-75 mobile stations per sector, 2% wireless channel error probability, 50% of mobile station performs handover at sector edge. It results in up to 130 kbps for downlink and up to 120 kbps for uplink generated traffic. When lowest rate modulation QPSK1/2x6 is used (it's most probable at sector edges) handover procedure can consume up to 18% and 41% sector capacity for downlink and uplink respectively. Therefore it's important to foresee what user expansion is expected in the future and initially implement required overhead.

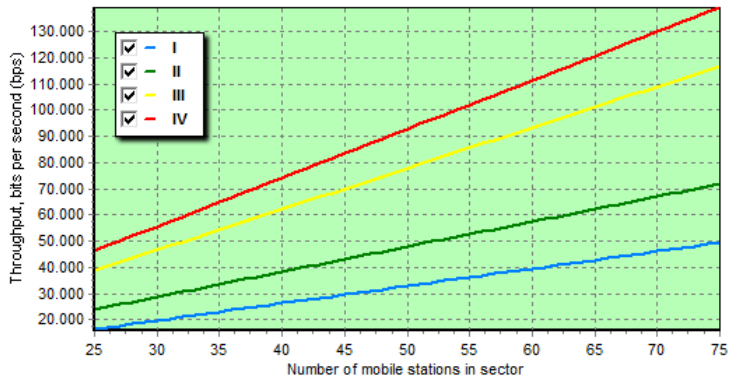

Figure 6. Handover data load dependencies from number of users by sector type

3. CONCLUSIONS

Software that is designed and presented by Authors allows automating network implementation and service simulation tasks for 4th generation wireless technologies. Software can be used as efficient tool for network providers or for educational purposes.

Example results presented in this paper show that multiple and complex tasks must be solved in order to achieve optimal network performance and even such regular procedure as handover can affect QoS. Automated software allows foreseeing and avoiding such of network behavior by choosing higher capacity equipment, selecting more efficient mobility management solutions or increasing BS density.

REFERENCES

[1] IEEE 802.16 Broadband Wireless Access Working Group, “Channel Models for Fixed Wireless Applications”, 2001 – p. 36.

[2] IEEE. “IEEE Standard for Local and Metropolitan area networks / Part 16: Air Interface for Broadband Wireless Access Systems” - New York, 2009 – p. 864.

THE DOUBLE AND TRIPLE RESONANCES INVESTIGATION FOR THE "CASSINI" LATTICE INTO THE DIELECTRIC

I. M. Petoev, V. A. Tabatadze, R. S. Zaridze

Tbilisi State University, Laboratory of Applied Electrodynamics,
3, Chavchavadze Ave. Tbilisi, Georgia
E-mail: ivanpetoev@gmail.com, E-mail: vasilitabatadze@gmail.com,
E-mail: revaz.zaridze@lae.tsu.ge

Abstract

The double and triple resonance effects for the certain metal – dielectric structure are studied. The structure represents the three dimensional periodic "Cassini" lattice inside of the usual dielectric with the finite sizes. The lattice element is a conductor wire with small electrical radius and with the form of the Cassini oval. Such structures have the interesting resonance properties in the wide frequency range, which makes it possible to present them as the complex materials. The program package was created and it gives the ability to study resonance properties of these structures. In the developed program package it is possible to change the parameters of the studied structure making advantage of numerical experiments.

1. INTRODUCTION

Investigation of the interaction between the electromagnetic field and periodic metal-dielectric structures is nowadays very topically problem because at some resonance frequencies these structures have the properties, similar to the complex materials [1-3]. The Method of Auxiliary Sources (MAS) gives ability to efficiently solve this kind of problems [4-8]. For this meaning there is the reason to increase the resonance effects in the system as much as it is possible.

As we know, at the resonance frequency, the amplitude of the excited current in the conductor element is higher. When the frequency is increased, after the resonance,

each element has a new undamped spectral mode, which creates a new additional lobe in the far zone. In case of the lattice, keeping the resonance frequency of the elements, at resonance distance between them, their electrodynamic interaction increases. As a result, because of the intensive mutual interaction the induced current increases sharply. This phenomenon is called "double" resonance. When the lattice is located inside of the ordinary dielectric, in some cases (at certain dielectric parameters with, "triple" and so on resonance), the resonance effects increase higher and in this case the system may have generally new interested properties, but in some special cases, similar to those of the complex materials like rotating polarization, negative reflections and so on.

The geometric form of the lattice element determines to which complex media corresponds given structure. For example, the structure of the elements with right or left chirality, embedded in the dielectric corresponds to the chiral media; if the lattice element represents two concentric split rings, then at certain frequencies this media has negative refractive index [3]. Each of these elements can be considered as the some small RLC circuit with high Q-factor. In this article is presented the investigation, when the lattice element has the form of the Cassini oval, which has the high Q-factor resonance properties in wide frequency range [4]. On resonance frequency the main incident field's energy reradiates to the perpendicular sides. From this point of view this study is novel.

The article consists of two main parts. In the first part is presented the problem statement and the method of solution. Here are considered two different cases, when the incident field source is located outside and inside of the considered dialectical structure. The MAS is used for the purpose to solve this electrodynamics problem. Based on the theoretical results program package was created for computer simulation. In the second part there are presented the numerical experiment results. As a first step, was studied the convergence of the calculation and its accuracy, which is dependent on the numbers of collocation points and the auxiliary parameters. After that we found the optimal parameters of some "Cassini lattice – dielectric" structures, when we have the "double" and "triple" resonance effects. Results of calculations are analysing.

2. THEORETICAL PART

2. 1. Problem statement and the method of solution. Let's consider a 3D Cassini lattice, with d_1, d_2, d_3 periods, inside of the usual dielectric. This dielectric, with known parameters ε, μ, has the finite size, enclosed by the S smooth surface (figure 1a)). The Cassini lattice element has small electrical radius ($dr_0 << \lambda$) and its mathematical equation in the polar coordinates is

$$\rho(\varphi) = \sqrt{c^2 \cos 2\varphi + \sqrt{a^4 - c^4 \sin^2 2\varphi}}\,,\ 0 \le \varphi \le 2\pi\,,$$

where $2c$ - represents the distance between the focuses, a - is the some parameter. In our case, there is the inequality $c < a < \sqrt{2}c$ and the element has four inflection points (figure 1b)).

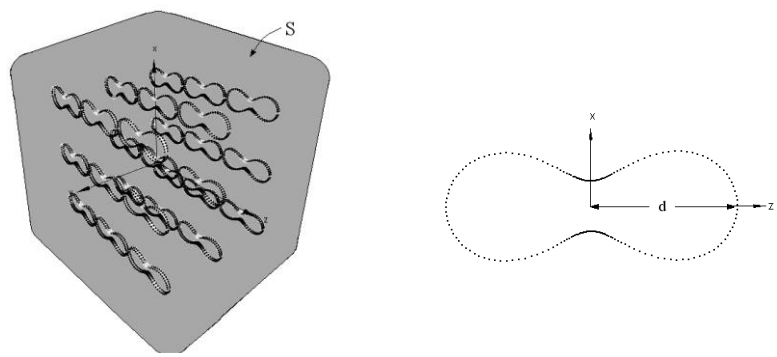

a) b)

Figure 1. a) Cassini lattice in the dielectric, b) The lattice element

Considered, the structure is exposed to the known harmonic $\vec{E}_{inc}(\vec{r})$, $\vec{H}_{inc}(\vec{r})$ incident field, with $e^{-i\omega t}$ time dependence (steady-state process). Here $\vec{r}$ is the radius-vector of the observation point. The source of this field is located in a certain point and has known polarization. Generally, it can be located outside, or inside of the studied system. If the source is located in the infinity, the incident wave is the plane. Mathematically, our problem is to find the diffraction field inside and outside of the structure as well as the field in the far zone.

2. 2. Solution of the problem. So, we are looking for the total inner $\vec{E}_{in}(\vec{r})$, $\vec{H}_{in}(\vec{r})$ and outer $\vec{E}_{out}(\vec{r})$, $\vec{H}_{out}(\vec{r})$ scattered fields. If the incident field source is located outside of the structure, then

$$\vec{E}_{in}(\vec{r}) = \vec{E}_2(\vec{r}) + \vec{E}_l(\vec{r}),\ \vec{H}_{in}(\vec{r}) = \vec{H}_2(\vec{r}) + \vec{H}_l(\vec{r}),$$

$$\vec{E}_{out}(\vec{r}) = \vec{E}_1(\vec{r}) + \vec{E}_{inc}(\vec{r}),\ \vec{H}_{out}(\vec{r}) = \vec{H}_1(\vec{r}) + \vec{H}_{inc}(\vec{r}).$$

If this source is located inside of the structure, then:

$$\vec{E}_{in}(\vec{r}) = \vec{E}_l(\vec{r}) + \vec{E}_2(\vec{r}) + \vec{E}_{inc}(\vec{r}),\ \vec{H}_{in}(\vec{r}) = \vec{H}_l(\vec{r}) + \vec{H}_2(\vec{r}) + \vec{H}_{inc}(\vec{r}),$$

$$\vec{E}_{out}(\vec{r}) = \vec{E}_1(\vec{r}),\ \vec{H}_{out}(\vec{r}) = \vec{H}_1(\vec{r}).$$

Here $\vec{E}_l(\vec{r})$, $\vec{H}_l(\vec{r})$ is the field, reradiated by the lattice; $\vec{E}_1(\vec{r})$, $\vec{H}_1(\vec{r})$ and $\vec{E}_2(\vec{r})$, $\vec{H}_2(\vec{r})$ are the fields scattered by the S surface outside and inside, respectively. Outer and inner total fields should satisfy the boundary conditions on the dielectric S surface and also along the σ surface of each lattice element. On the S surface, total field tangential component continuity is required. This condition should be satisfied for any tangential component on the S. If it is satisfied along two perpendicular tangential $\vec{\tau}_1$ and $\vec{\tau}_2$ vectors, then it will be satisfied along any others (figure 2a)). So:

$$\begin{cases} \vec{E}_{in}(\vec{r}_S)\cdot\vec{\tau}_1 = \vec{E}_{out}(\vec{r}_S)\cdot\vec{\tau}_1, & \vec{H}_{in}(\vec{r}_S)\cdot\vec{\tau}_1 = \vec{H}_{out}(\vec{r}_S)\cdot\vec{\tau}_1, \\ \vec{E}_{in}(\vec{r}_S)\cdot\vec{\tau}_2 = \vec{E}_{out}(\vec{r}_S)\cdot\vec{\tau}_2, & \vec{H}_{in}(\vec{r}_S)\cdot\vec{\tau}_2 = \vec{H}_{out}(\vec{r}_S)\cdot\vec{\tau}_2. \end{cases} \tag{1}$$

Along the lattice element's surface total electric field's tangential component must be:

$$\vec{E}_{in}(\vec{r}_\sigma)\cdot\vec{\tau} = 0, \tag{2}$$

where $\vec{\tau}$ is the tangential vector along the Cassini element (figure 2b)).

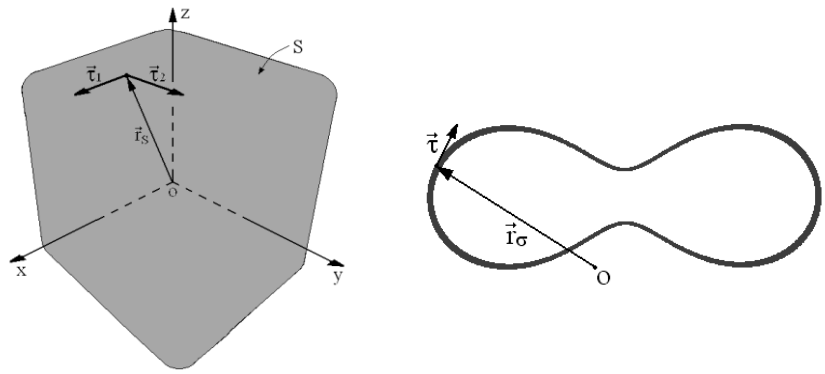

a) b)

Figure 2. a) Tangentials on the dielectric surface, b) Tangential on the Cassini element

To find the $\vec{E}_l(\vec{r})$, $\vec{H}_l(\vec{r})$ reradiated field's expression the lattice elements are divided on small segments. The length of each segment should be small enough to consider current as constant along this segment. Using the method of potentials we get:

$$\vec{E}_l(\vec{r}) = \sum_{\alpha,\beta,\gamma}\sum_{n=1}^{N} I_{\alpha\beta\gamma,n}\hat{L}G\left(\vec{r},\vec{r}_{\alpha\beta\gamma,n}\right),\ \vec{H}_l(\vec{r}) = (1/4\pi)\sum_{\alpha,\beta,\gamma}\sum_{n=1}^{N} I_{\alpha\beta\gamma,n}\nabla\times G\left(\vec{r},\vec{r}_{\alpha\beta\gamma,n}\right)\Delta\vec{l}_{\alpha\beta\gamma,n}, \quad (3)$$

$$\hat{L}G\left(\vec{r},\vec{r}_{\alpha\beta\gamma,n}\right) = \left(i/4\pi\omega\varepsilon_0\varepsilon\right)\left\{k^2 G\left(\vec{r},\vec{r}_{\alpha\beta\gamma,n}\right)\Delta\vec{l}_{\alpha\beta\gamma,n} - \nabla\left[G\left(\vec{r},\vec{r}^{+}_{\alpha\beta\gamma,n}\right) - G\left(\vec{r},\vec{r}^{-}_{\alpha\beta\gamma,n}\right)\right]\right\},$$

$$G\left(\vec{r},\vec{r}_{\alpha\beta\gamma,n}\right) = e^{ik\left|\vec{r}-\vec{r}_{\alpha\beta\gamma,n}\right|}\Big/\left|\vec{r}-\vec{r}_{\alpha\beta\gamma,n}\right|.$$

where $\alpha\beta\gamma$ - are the numbers of the lattice's elements (along each axes, respectively, because we consider 3D lattice), $n = 1, 2, ..., N$ - the number of the segment; $I_{\alpha\beta\gamma,n}$ - the unknown amplitude of the induced current, flowing in the $\Delta l_{\alpha\beta\gamma,n}$ segment; $k = \omega\sqrt{\varepsilon_0\mu_0\varepsilon\mu}$ is a wave number inside of the system; $\vec{r}_{\alpha\beta\gamma,n}$, $\vec{r}^{+}_{\alpha\beta\gamma,n}$, $\vec{r}^{-}_{\alpha\beta\gamma,n}$ and $\Delta\vec{l}_{\alpha\beta\gamma,n} = \vec{r}^{+}_{\alpha\beta\gamma,n} - \vec{r}^{-}_{\alpha\beta\gamma,n}$ vectors show the segment position and orientation in the space (figure 3).

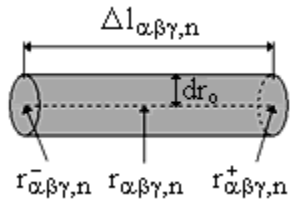

Figure 3. Segment's geometry

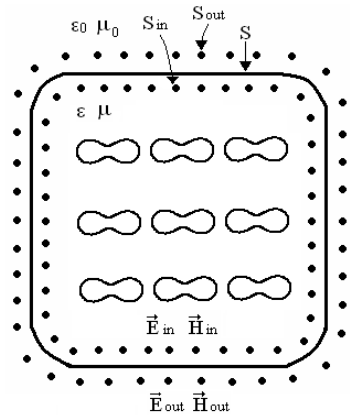

Figure 4. The MAS application

The MAS is used in order to find the unknown $\vec{E}_1(\vec{r})$, $\vec{H}_1(\vec{r})$ and $\vec{E}_2(\vec{r})$, $\vec{H}_2(\vec{r})$ fields. Two smooth auxiliary surfaces S_{in}, S_{out} are constructed from both side of the dielectric, considering scattered field singularities and the combined auxiliary sources are distributed on each of them (figure 4).

The number of auxiliary sources must be equal to the number of points located on the dielectric S surface, where the boundary conditions (1) are to be satisfied. In order to take into account all kind of polarization two mutual perpendicular combined dipoles are chosen as the auxiliary sources. The polarization vectors of these dipoles have the tangential direction $\vec{\tau}_1$ and $\vec{\tau}_2$ in each point of the auxiliary surface. The outer $\vec{E}_1(\vec{r})$, $\vec{H}_1(\vec{r})$ fields are described using inner auxiliary sources:

$$\vec{E}_1(\vec{r}) = \sum_{p,q}\left(A_{pq}\vec{E}^{pq}_{in,\tau_1}(\vec{r}) + B_{pq}\vec{E}^{pq}_{in,\tau_2}(\vec{r})\right),\ \vec{H}_1(\vec{r}) = \sum_{p,q}\left(A_{pq}\vec{H}^{pq}_{in,\tau_1}(\vec{r}) + B_{pq}\vec{H}^{pq}_{in,\tau_2}(\vec{r})\right). \quad (4)$$

Inner $\vec{E}_2(\vec{r})$, $\vec{H}_2(\vec{r})$ field s are described by outer auxiliary sources:

$$\vec{E}_2(\vec{r}) = \sum_{f,g}\left(C_{fg}\vec{E}^{fg}_{out,\tau_1}(\vec{r}) + D_{fg}\vec{E}^{fg}_{out,\tau_2}(\vec{r})\right),\ \vec{H}_2(\vec{r}) = \sum_{f,g}\left(C_{fg}\vec{H}^{fg}_{out,\tau_1}(\vec{r}) + D_{fg}\vec{H}^{fg}_{out,\tau_2}(\vec{r})\right). \quad (5)$$

Here pq and fg indexes show the number of auxiliary source, the out and in indexes determine on which auxiliary surface is located dipole, the τ_1 and τ_2 indexes show its orientation. Each auxiliary source (two perpendicular combined dipoles in our case) has two unknown amplitudes. The field of the combined dipole is defined as:

$$\vec{E}(\vec{r}) = \vec{E}_{el}(\vec{r}) + \sqrt{\mu_0\mu/\varepsilon_0\varepsilon}\vec{E}_{mag}(\vec{r}),\ \vec{H}(\vec{r}) = \vec{H}_{el}(\vec{r}) + \sqrt{\mu_0\mu/\varepsilon_0\varepsilon}\vec{H}_{mag}(\vec{r}),$$

where $\vec{E}_{el}(\vec{r})$, $\vec{H}_{el}(\vec{r})$ and $\vec{E}_{mag}(\vec{r})$, $\vec{H}_{mag}(\vec{r})$ - are the fields of the electric and magnetic dipoles:

$$\vec{E}_{el}(\vec{r}) = \left(e^{ikR}/4\pi\varepsilon_0\varepsilon\right)\left\{\left(1/R^3 - ik/R^2\right)\left[3\vec{R}_0\cdot\left(\vec{R}_0\cdot\vec{p}_{el}\right) - \vec{p}_{el}\right] - \left(k^2/R\right)\left(\vec{R}_0\times\left(\vec{R}_0\times\vec{p}_{el}\right)\right)\right\},$$

$$\vec{H}_{el}(\vec{r}) = \left(\omega e^{ikR}/4\pi\right)\left(k/R + i/R^2\right)\left(\vec{R}_0\times\vec{p}_{el}\right),$$

$$\vec{E}_{mag}(\vec{r}) = \left(k^2 e^{ikR}/4\pi\right)\left(1/R^2 - ik/R\right)\left(\vec{p}_{mag}\times\vec{R}_0\right),$$

$$\vec{H}_{mag}(\vec{r}) = \left(e^{ikr}/4\pi\right)\left\{\left(1/R^3 - ik/R^2\right)\left[3\vec{R}_0\cdot\left(\vec{R}_0\cdot\vec{p}_{mag}\right) - \vec{p}_{mag}\right] - \left(k^2/R\right)\left(\vec{R}_0\times\left(\vec{R}_0\times\vec{p}_{mag}\right)\right)\right\},$$

where $\vec{R}_0 = \left(\vec{r} - \vec{r}_j\right)/\left|\vec{r} - \vec{r}_j\right|$, $R = \left|\vec{r} - \vec{r}_j\right|$, $\vec{r}_j$ - is the dipole radius-vector, $\vec{p}_{el}$ and $\vec{p}_{mag}$ - are the polarization vectors.

So the problem is to find unknown amplitudes of the auxiliary sources: A_{pq}, B_{pq}, C_{fg}, D_{fg} and the amplitudes of currents $I_{\alpha\beta\gamma,n}$ induced in the lattice elements. In this case we suppose that wire's electric radius is small and current value's redistribution along the cross-sections is negligible. These amplitudes we can find from the boundary conditions satisfaction (1), (2), which are the systems of linear equations. If the incident field source is located outside of the considered structure, the equations system has form:

$$\begin{cases}\left(\vec{E}_2(\vec{r}_\sigma) + \vec{E}_l(\vec{r}_\sigma)\right)\cdot\vec{\tau} = 0\\ \left(\vec{E}_2(\vec{r}_S) - \vec{E}_1(\vec{r}_S) + \vec{E}_l(\vec{r}_S)\right)\cdot\vec{\tau}_1 = \vec{E}_{inc}(\vec{r}_S)\cdot\vec{\tau}_1\\ \left(\vec{E}_2(\vec{r}_S) - \vec{E}_1(\vec{r}_S) + \vec{E}_l(\vec{r}_S)\right)\cdot\vec{\tau}_2 = \vec{E}_{inc}(\vec{r}_S)\cdot\vec{\tau}_2\\ \left(\vec{H}_2(\vec{r}_S) - \vec{H}_1(\vec{r}_S) + \vec{H}_l(\vec{r}_S)\right)\cdot\vec{\tau}_1 = \vec{H}_{inc}(\vec{r}_S)\cdot\vec{\tau}_1\\ \left(\vec{H}_2(\vec{r}_S) - \vec{H}_1(\vec{r}_S) + \vec{H}_l(\vec{r}_S)\right)\cdot\vec{\tau}_2 = \vec{H}_{inc}(\vec{r}_S)\cdot\vec{\tau}_2,\end{cases}$$

and for $\vec{E}_l$, $\vec{H}_l$, $\vec{E}_1$, $\vec{H}_1$, $\vec{E}_2$, $\vec{H}_2$ fields we must use (3) - (5) formulas. When the incident field source is located inside of structure, then we will have

$$\begin{cases} \left(\vec{E}_l\left(\vec{r}_\sigma\right)+\vec{E}_2\left(\vec{r}_\sigma\right)\right)\cdot\vec{\tau}=-\vec{E}_{inc}\left(\vec{r}_\sigma\right)\cdot\vec{\tau} \\ \left(\vec{E}_l\left(\vec{r}_S\right)+\vec{E}_2\left(\vec{r}_S\right)-\vec{E}_1\left(\vec{r}_S\right)\right)\cdot\vec{\tau}_1=-\vec{E}_{inc}\left(\vec{r}_S\right)\cdot\vec{\tau}_1 \\ \left(\vec{E}_l\left(\vec{r}_S\right)+\vec{E}_2\left(\vec{r}_S\right)-\vec{E}_1\left(\vec{r}_S\right)\right)\cdot\vec{\tau}_2=-\vec{E}_{inc}\left(\vec{r}_S\right)\cdot\vec{\tau}_2 \\ \left(\vec{H}_l\left(\vec{r}_S\right)+\vec{H}_2\left(\vec{r}_S\right)-\vec{H}_1\left(\vec{r}_S\right)\right)\cdot\vec{\tau}_1=-\vec{H}_{inc}\left(\vec{r}_S\right)\cdot\vec{\tau}_1 \\ \left(\vec{H}_l\left(\vec{r}_S\right)+\vec{H}_2\left(\vec{r}_S\right)-\vec{H}_1\left(\vec{r}_S\right)\right)\cdot\vec{\tau}_2=-\vec{H}_{inc}\left(\vec{r}_S\right)\cdot\vec{\tau}_2. \end{cases}$$

Unknown amplitudes are determined by numerical simulation. Then the outer and inner scattered fields can be calculated in any point, including in infinity (patterns).

3. RESULTS OF THE NUMERICAL EXPERIMENTS

3. 1. Calculation accuracy testing. Previous to study electrodynamic properties of the system was tested values of some auxiliary parameters to get good accuracy of calculations. Besides, note that the numerical results are presented in the units of the maximal radius *d* of the Cassini oval (figure 1b)). Therefore, these results are valid in wide frequency range, where Maxwell's equation system can be used. Because we are restricted in the size of this paper, we provide only some part of the results.

Figure 5 shows error dependence on the auxiliary parameter dr_0, which geometrically is a wire radius. The incident field is a plane wave. It propagates along OY direction and has both OX and OZ polarization. Here are three curves, when there are 8, 16 and 32 auxiliary sources along wavelength. As we can see, to get error smaller 20%, we need to have at least 32 sources. This number is required due to the complicated geometry. Investigation shows, that the optimal wire radius is $dr_0 = 0.083d$, when in case of 32 auxiliary sources the error is 10%. If $dr_0 > 0.083d$, the error is smaller 10%, but the characteristic becomes nonphysical, because the current, in our case, cannot describe the angular dependence of the wire's cross section.

In figure 6 we can see the boundary condition satisfaction along the certain wire's AB part normalised on the maximum one. We can see that the error of the solution becomes smaller, when the number of auxiliary sources increases. In the concave part of the wire, the error is negligible. So we don't consider this part. All presented numerical results valid with 10-15% acc

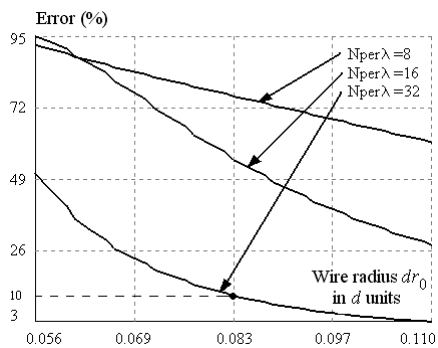

Figure 5. Error dependence on the auxiliary parameter

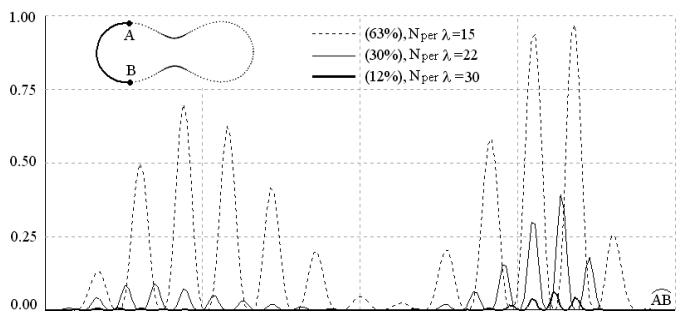

Figure 6. The boundary condition satisfaction along the element

3. 2. One element investigation (plane incident wave). At first was considered just one Cassini oval and was investigated its electrodynamic properties. The incident field is a plane wave, propagates along OY direction and has equal OX and OZ polarization. Figure 7 shows current maximum dependence on the kd parameter, where k is a wave number. Here we can see two curves which correspond to different geometries of oval (figure 8). Here a and c are the oval parameters (see the curve equation in theoretical part). The maximums on these curves correspond to the resonance frequencies. In case of $a = 1.02c$ the resonance is shifted. Figure 9 and 10 shows the near field's E_z component distribution and far field's pattern when $a = 1.02c$ in case of resonance ($kd = 4.36$). As we can see, the main part of reradiated field has OY direction. The investigation of the field's polarization properties shows, that in case of one element the reradiated field has elliptical polarization with ellipticity 1:2.5.

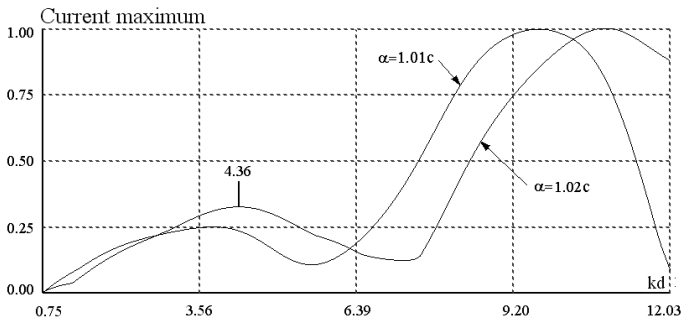

Figure 7. Current maximum dependence on the *kd*

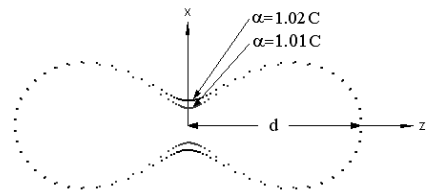

Figure 8. Cassini geometry

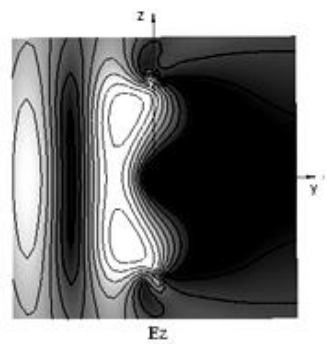

Figure 9. Near field's E_z component distribution

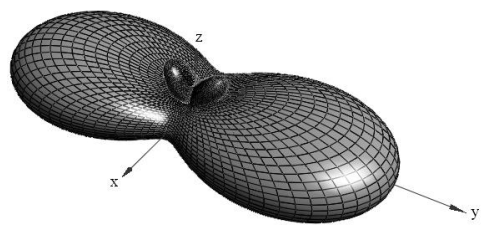

Figure 10. Far field's pattern

3. 3. One element investigation. Next was considered the case, when the incident field source represents the combined dipole with OX polarization, located in point $(0,-3d,0)$. Figure 11 shows the normalized reflected power dependence on the kd parameter. The peaks on this curve correspond to the resonance. On the figure 12, 13 are presented far field's pattern and the near field's E_z component distribution, when $kd = 1.79$. As we can see, the main part of the energy propagates along OY axis and along his opposite direction. When the incident field has OZ polarization, dependent between the reflected power and kd parameter has the form (figure 14). Investigation shows, that the reflected power is ten times bigger, than OX polarization case. Figure 15 and 16 shows the far field's pattern and the near field's distribution in case of resonance $kd = 6.195$. Here also the main part of the energy propagates along OY axis and along his opposite direction.

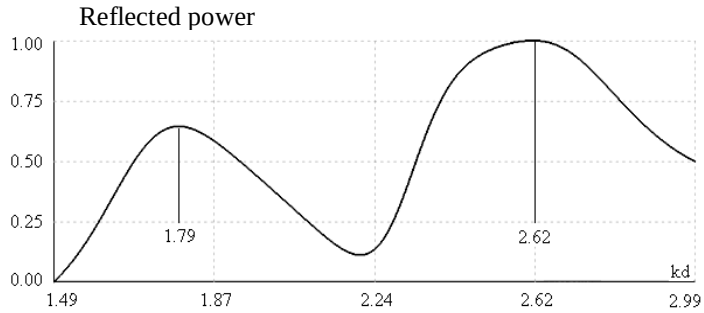

Figure 11. Normalized reflected power dependence on the *kd* parameter

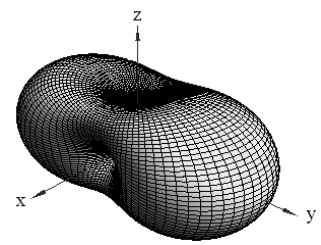

Figure 12. Far field's pattern

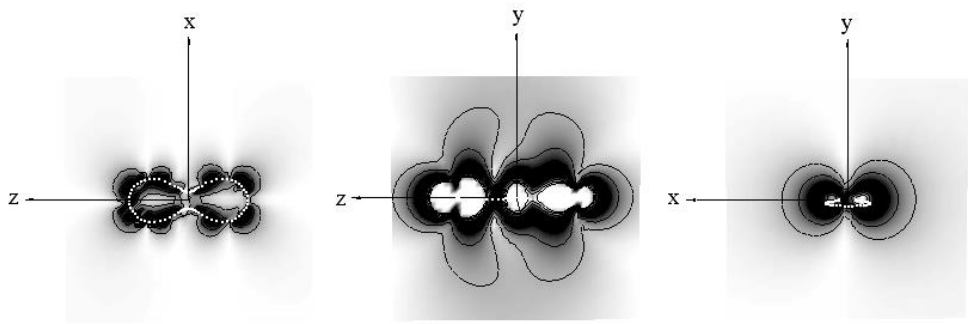

Figure 13. The near field's *Ez* component distribution (*kd*=1.79)

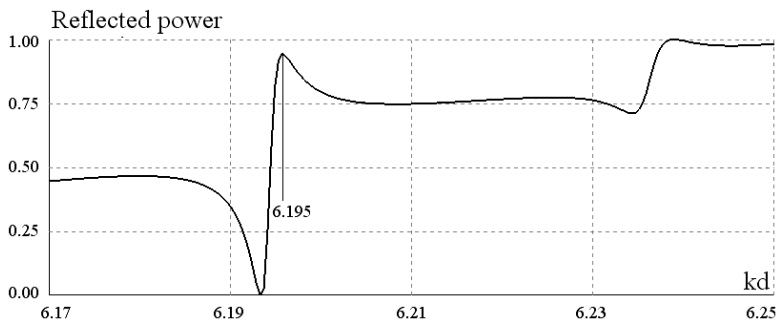

Figure 14. Normalized reflected power dependence on the *kd* parameter

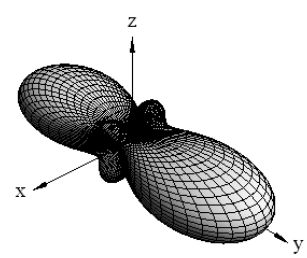

Figure 15. Far field's pattern

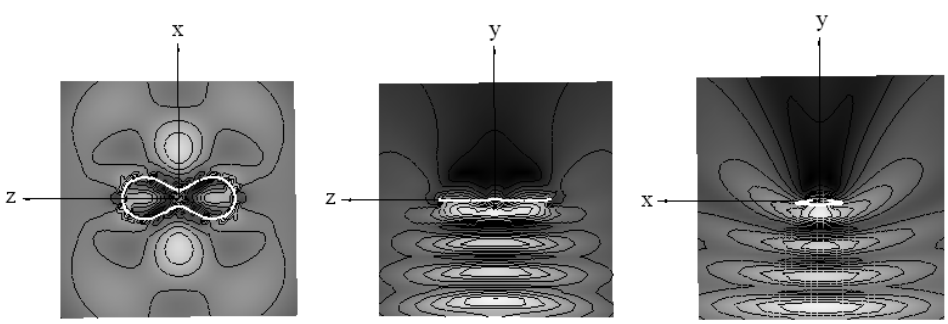

ide

Figure 16. The near field's *Ez* component distribution (*kd*=6.195)

If we change the geometrical form of Cassini element, we can get more wide resonance. On figure 17, the middle part of the Cassini element is less concave ($a = 1.1c$). The incident field source has coordinates $(4d, 0, 0)$, propagates along opposite of the OX direction and has OZ polarization. In the range from $kd = 2.3340$ to $kd = 6.2240$, the element has wide resonance (figure 18). On the figure 19 a) and we can see the far field's pattern in case of resonance. In this case, the scattered field has circular polarization (figure. 19 b)), which is shown better in animation. The scattered field has two big lobs. The near field's components distribution in this case is shown on the figure 20.

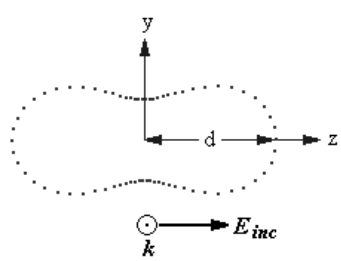

Figure 17. The Geometry of Cassini element

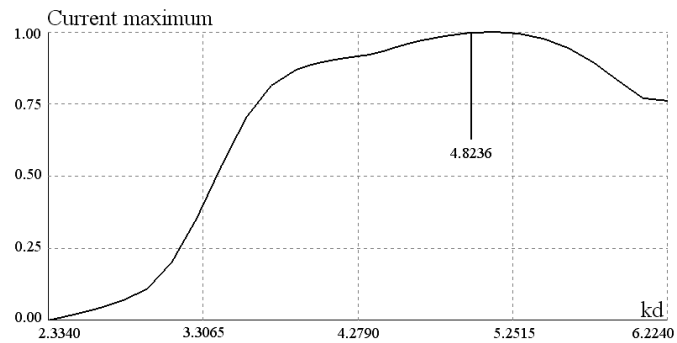

Figure 18. The current maximum dependence on *kd* parameter

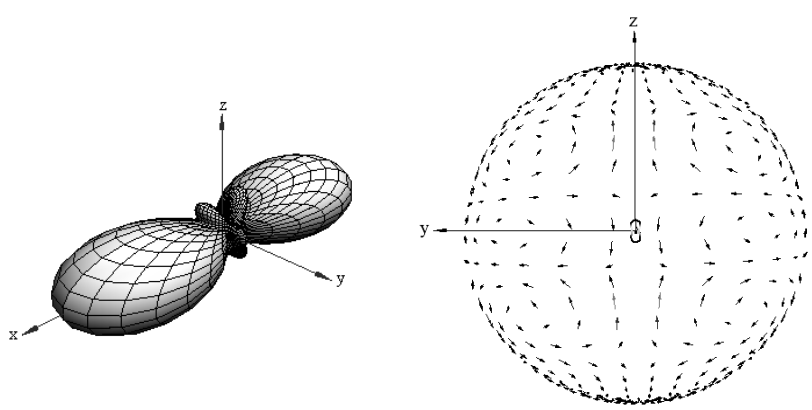

a) b)

Figure 19. a) Far field's pattern (*kd*=4.8236), b) polarization rotation

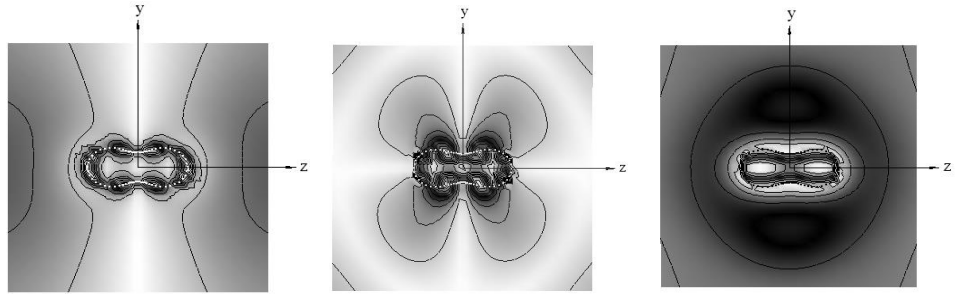

Figure 20. Near field's components distribution

3. 4. Investigation the lattice with Cassini elements (plane incident wave). Next was considered the lattice with periods $d_1 = d_2 = d_3 = 2.09d$ (figure 21). The number of elements is 27 and along each axis are three one. The incident field is a plane wave, propagates along OY direction and has equal OX and OZ polarization. Figure 22 shows reflected power dependence on the kd parameter. When we change the parameters of Cassini oval, as it was in case of one element (figure 7) here we can see, the resonances are amplified but not shifted.

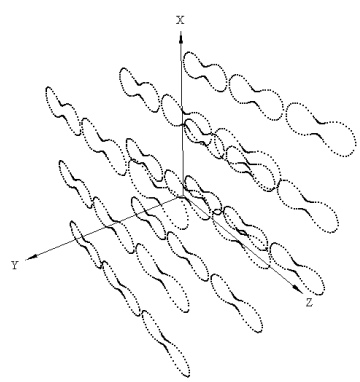

Figure 21. The lattice geometry

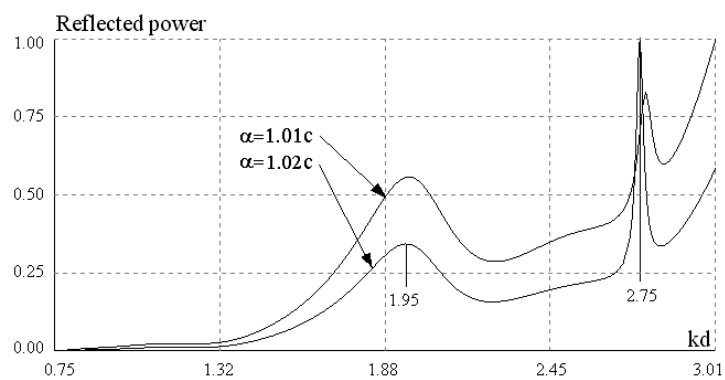

Figure 22. Reflected power dependence on the *kd* parameter

The figures 23-26 show the far field's pattern and near field's distribution, when $a = 1.02c$, in resonance cases ($kd = 1.95$ and $kd = 2.75$). At the resonance $kd = 1.95$ we see that the main part of the reradiated field propagates along OY direction. At the next $kd = 2.75$ resonance there are several special direction of radiation in XOY plane section. The investigation of the field polarization properties shows, that in case of lattice, the reradiated field has elliptical polarization with ellipticity 1:2.

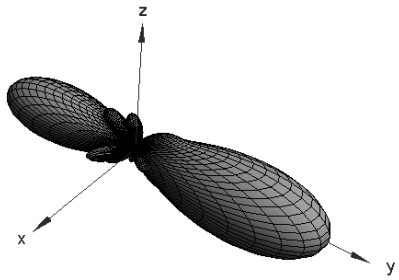

Figure 23. Far field's pattern *kd*=1.95

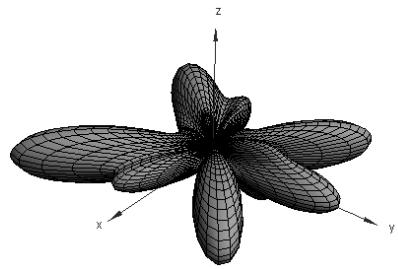

Figure 24. Far field's pattern *kd*=2.75

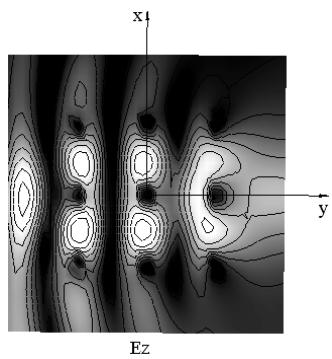

Figure 25. Near field's E_z component distribution (*kd*=1.95)

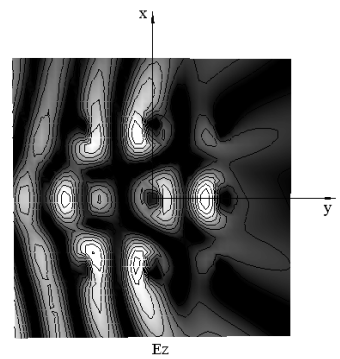

Figure 26. Near field's E_z component distribution (*kd*=2.24)

3. 5. Investigation the lattice with Cassini elements. Next was studied the system with three Cassini elements in free space (figure 27). The incident field combined source has coordinates $(0,-3d,0)$ and OX polarization. At the value $kd=1.79$ - which represents the resonance value of the one element (see figure 11), was found the resonance distance between them ($d_2=0.714d$). Figure 28 and 29 shows the far field's pattern and the near field's E_z component distribution in case of double resonance.

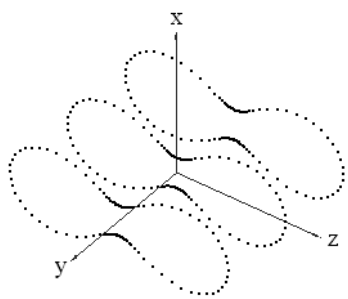

Figure 27. The structure geometry

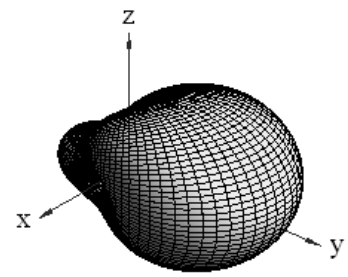

Figure 28. Far field's pattern

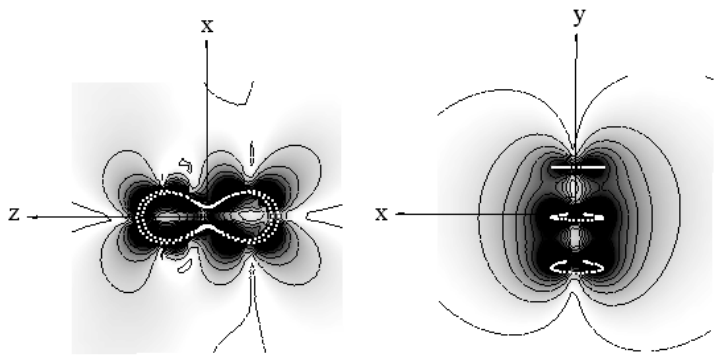

Figure 29. Near field's distribution in case of double resonance

The main part of the energy propagates along OY direction. The pattern will be more directed if the incident field has OZ polarization. At the resonance value $kd = 6.195$ (see figure 14) were found two values of the distance between the elements, when we have double resonance ($d_2 = 0.04d$ and $d_2 = 0.84d$). On the figures 30 and 31 we can see the near field's E_z component distribution and far field's pattern.

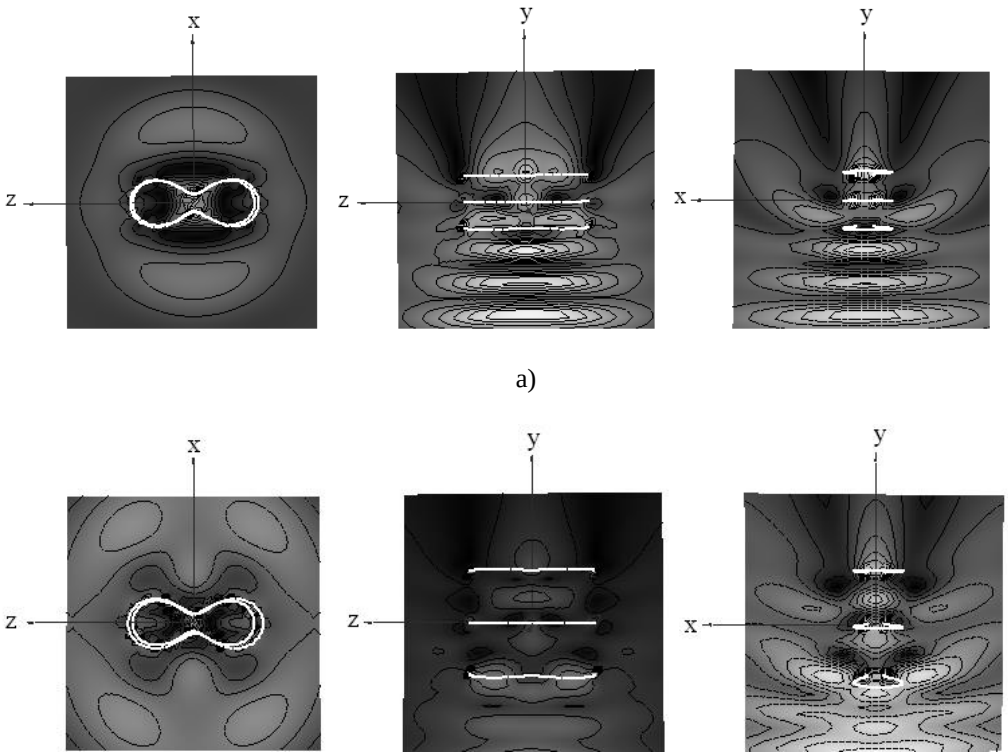

a)

b)

Figure 30. Near field's distribution: a) $d_2 = 0.04d$, b) $d_2 = 0.84d$

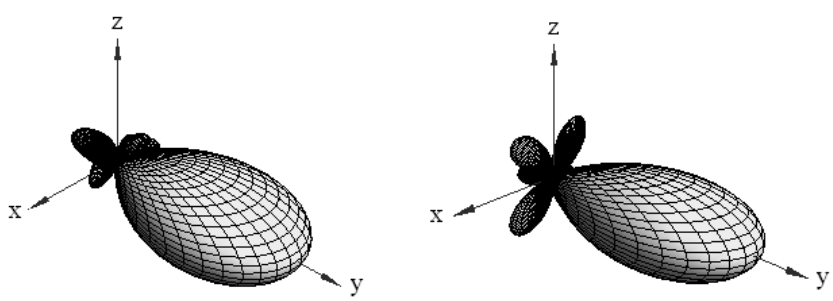

a) b)

Figure 31. Far field's pattern: a) $d_2 = 0.04d$, b) $d_2 = 0.84d$

3. 6. Lattice inside of the dielectric. Also was considered the case, when three Cassini elements are bounded in dielectric parallelepiped, with parameters $\varepsilon = 4, \mu = 1$. The distance between the elements is $d_2 = 1.53d$. The dielectric has smooth surface with sizes $2.37d \times 2.79d \times 4.87d$ and with $R = 0.56d$ - radius of the curvature (figure 32). Here also the incident field is a plane wave, propagates along OY direction and has equal

OX and OZ polarization. Figure 33 shows the normalized reflected power dependence on the kd parameter. Here we have two curves for different distances between the elements. As we see, the reflected power increases, if the distance is $d_2 = 2.09d$. Figure 34 shows the near field distribution in case of resonance $kd = 1.2075$.

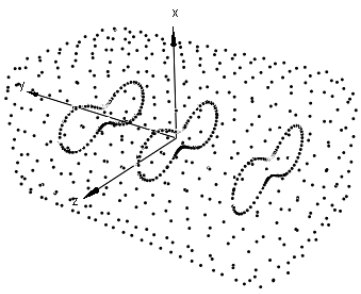

Figure 32. Cassini elements inside of the dielectric

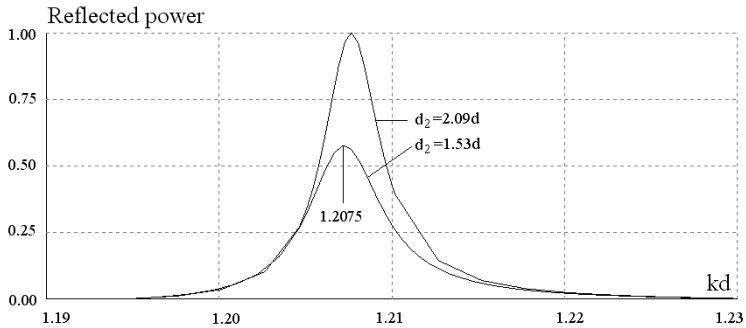

Figure 33. Reflected power dependence on the *kd* parameter

The investigation of the field polarization properties shows, that in case of dielectric, the reradiated field has practically circular polarization.

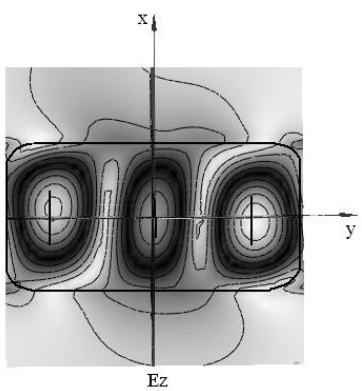

Figure 34. The near field's distribution when *kd* =1.2075

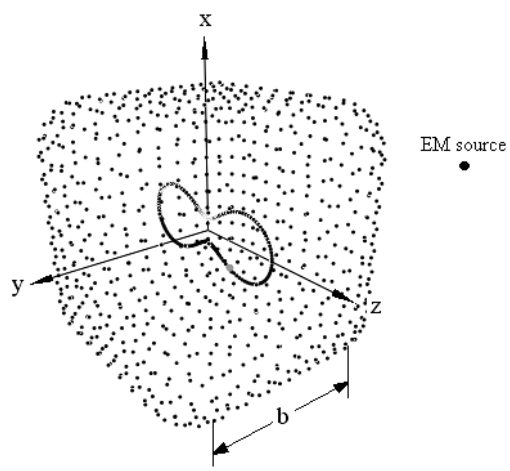

Figure 35. Cassini in dielectric cube

Next was considered the case, when the incident field source represents the combined dipole and is located near of the structure in point $(0, -4d, 0)$. The structure represents just one Cassini element inside of the dielectric cube (figure 35).

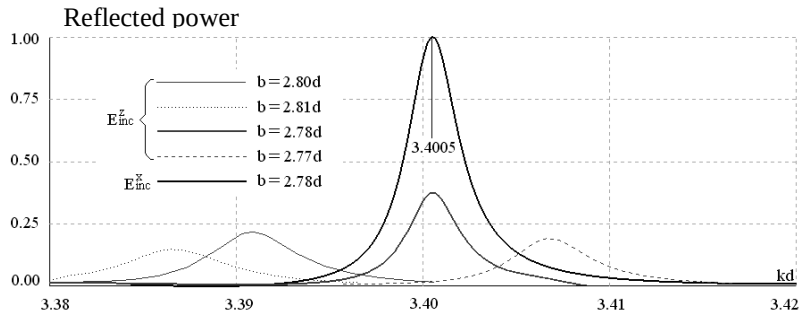

Figure 36. Reflected power dependence on *kd* parameter

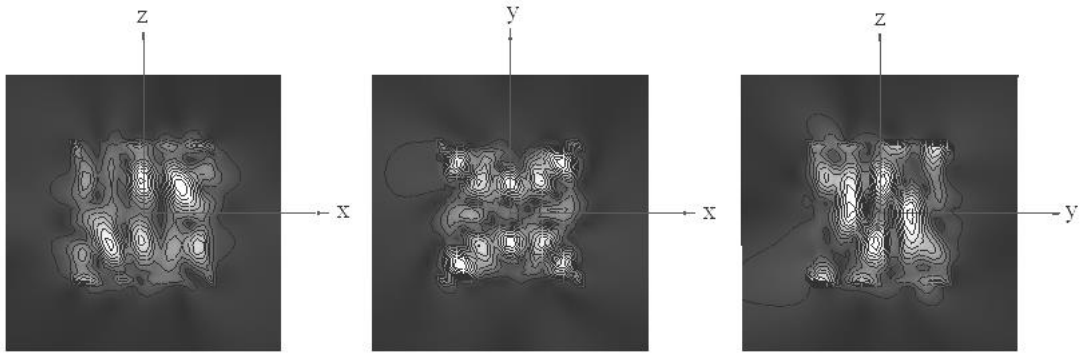

Figure 37. Near field's distribution

Figure 36 shows the normalized reflected power dependence on the kd parameter. These curves are for different cube b sizes. When the incident field has E_{inc}^{x} component, we have highest interaction between the Cassini - cube, which means the double resonance of this structure (the solid black line). On the figure 37 we can see the near field's E_z component distribution in case of the resonance ($kd = 3.4005$).

4. CONCLUSION

In this article there was considered the investigation of the electrodynamic properties of: one "Cassini" shape wire; the lattice of this "Cassini" shape elements in free media and also, embedded the lattice into the dielectric. Numerical experiments showed that Cassini has wide resonance and in some cases the scattered field has an elliptical polarization, which gives practical possibility to create artificial chiral media in the wide frequency range. "Double", "triple" resonances of such system were study.

When the elements are embedded in the dielectric, if we correctly choose the parameters of the elements and the distance between them, we can sharply increase the resonance properties of the system.

ACKOWLEDGMENT

This study was performed under World Federation of Scientists & Georgian Scholarship Program. Also, the authors thank the reviewers for their comments and suggestions.

REFERENCES

[1]. N. Engheta, R. W. Ziolkowski. Metamaterials, Physics and Engineering Explorations. IEEE Press, Wiley Interscience, 2006.

[2]. G. V. Eleftheriades, K. G. Balmain “Negative-Refraction Metamaterials fundamental principles and applications”, A John Willey & Sons, Inc., Publication, New Jersey, 2005.

[3]. I. V. Lindell, A. H. Sihvola, S. A. Tretyakov and A. J. Viitanen. Electromagnetic Waves in Chiral and Bi-Isotropic Media (Artech House, Boston, 1994).

[4]. R. Zaridze, D. Karkashadze and J. Khatiashvili, "The Method of Auxiliary Sources for Investigation of Along-Regular Waveguides", Tbilisi State University Publisher, p.150, Tbilisi, 1985.

[5] Popovidi-Zaridze R. S., Tsverikmazashvili Z. S. Numerical solution of diffraction problem by modified method of non-orthogonal series," Journal of Applied Mathematics and Mathematical Physics, Moscow, 1977, pp. 384-393, in Russian (English translation available, translated and reprinted by Scientific Translation Editor, Oxford, 1978).

[6]. R. Zaridze and G. Talakvadze, "Investigation of Resonance Characteristics of a Lattice of Metal Cylinders with Dielectric layer of finite width", Radiotechnics and Electronics, No.1, Moscow, 1981.

[7]. R. Zaridze, G. Bit-Babik, K. Tavzarashvili at al. "Wave Field Singularity Aspects Large-Size Scatterers and Inverse Problems." IEEE Transactions on Antennas and Propagation 50, No. 1, 50, (January 2002). http:// lae.tsu.ge/mas/AP_Trans2002.pdf

[8]. V. Tabatadze, A. Bijamov, Jr. D, Kakulia at al. "Design and Analysis of Planar Photonic Band Gap Devices". International Journal of Infrared and Millimetre Waves. (August 22, 2008). http:// lae.tsu.ge/mas/P2008Z.pdf

EXPERIMENTAL STUDY OF THE INFLUENCE OF AEROSOL PARTICLES ON LINK RANGE OF FREE SPACE LASER COMMUNICATION SYSTEM IN IRAQ

J. M. Jassim , A. K. Kodeary

Babylon University - College of Science for Women, Iraq
e-mail : jassimm2007@yahoo.com.

Abstract
Attenuation due to aerosols restricts the distance of FSO communication systems and limits the availability for line-of-sight terrestrial link. This work is focused on the effect of aerosols on the FSO link. The attenuations was studied in the Hilla city in the aerosols phenomena for three selected wavelengths (532, 1064, and 10600 nm) for horizontal transmitting range (1-10) Km. The results show that system availability as a function of the range, and indicate that FSO systems can be deployed with reliability in Hilla city of Iraq.

Key words: Attenuation, Propagation, Atmospheric Transmittance, FSO.

1. INTRODUCTION

The propagation of electromagnetic (EM) wave in the atmosphere is subject to many effects, that happen when the interaction between the EM wave and the field environment in a complex mechanism which can be cover the propagation of EM wave in different ranges starting with x-ray and ending to radio wave. Laser as a from of EM wave unavoidable suffers all of these effects, which such as dense fog, haze, dust, rain, clouds, eddies and air molecules which are unavoidable effects on the laser beam [1].
The propagation of laser beam through atmospheric space can be classified in horizontal, vertical, or slant paths propagation which may provide an information on structure of the atmosphere [2].

2. ATMOSPHERIC ATTENUATION

The attenuation of laser power in the atmosphere is described By Beer's Lambert law [3].

$$\tau(R) = \frac{P_r}{P_t} = e^{-\mu R} \qquad (1)$$

where: $\tau(R)$ =transmittance at range R, P_r = laser power at R , P_t = laser power at the source, at zero range μ =Attenuation or total extinction coefficient (per unit length).
The attenuation coefficient has contributions from the absorption and scattering of laser photons by different aerosols and gaseous molecule in the atmosphere [4]. The attenuation coefficient is made up of four parts:

$$\mu = \alpha_g + \alpha_p + \gamma_g + \gamma_p \qquad (2)$$

where: α_g = molecular absorption coefficient, α_p = aerosol absorption

coefficient, γ_g =molecular or Rayleigh scattering coefficient, and γ_P =aerosol or Mie scattering coefficient.

This relationship applies to both visible and IR wavelengths, in this expression, the factor $e^{-\mu R}$ represent the transmittance.

The total atmospheric transmittance can be factored as the product of the absorption and scattering transmittances

$$\tau(R) = \tau(\alpha)\tau(s) \qquad (3)$$

where: τ_α = the absorption transmittance, τ_s = the scattering transmittance [4].

3. ATTENUATION DUE TO DUST

Dust is a solid particle formed by disintegration processes such as crushing, grinding, blasting, and drilling. The particles are small replicas of the parent material, and their particle size may range from submicroscopic to microscopic. The attenuation from dust and atmospheric aerosols are resulting from Mie scattering particles, which dependent on the volume of the atmospheric aerosols, and the effects of absorption electromagnetic will be relatively small comparing with Mie scattering, therefore, the scattering coefficient can be computed form the visibility distance and wavelength of the incident beam [5-7]. The range of visibility is related with concentration of dust as:

$$V = 7080 \times C^{-0.8} \qquad (4)$$

where V - visibility distance ,
C- concentration of dusts (various with altitude) Therefore, there is a direct relation between concentrations of dust and scattering coefficient due to atmospheric aerosol is [8]:

$$\tau_S = \exp\left[\left(\frac{-3.91}{7080 \times C^{-0.8}}\right)\left(\frac{\lambda}{0.55}\right)^{-q} \times R\right] \qquad (5)$$

where τ_S - transmittance resulting from scattering , λ - wavelength , q - positive constant proposed computed (the size distribution of the scattering particles) ,
R - propagation range .

4. RESULTS AND DISCUSSION

4.1. Calculation of the atmospheric transmittance for three different beams propagation in Hilla city

Figures (1),(2), and (3), which represent variations of atmospheric transmittance with range of 1 km, for wavelengths of (532, 1064, and 10600 nm), for state of clear weather, haze weather, and thick fog weather. In this figure its found that the wavelength of 10600 nm more capability to penetrate atmospheric effects on beam

propagation beam than other wavelengths, because higher wavelength, and found that wavelength of 1064 nm is better than 532 nm.

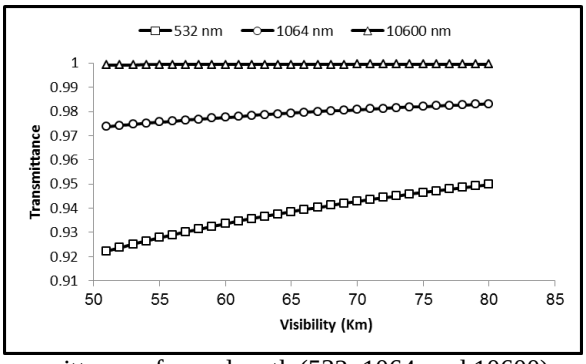

Figure 1. Atmospheric transmittance of wavelength (532, 1064, and 10600) nm dependent on visibility distance for very clear weather.

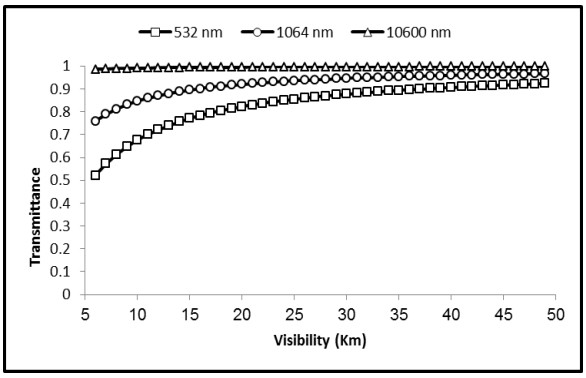

Figure 2. Atmospheric transmittance of wavelength (532, 1064, and 10600) nm dependent on visibility distance for haze weather.

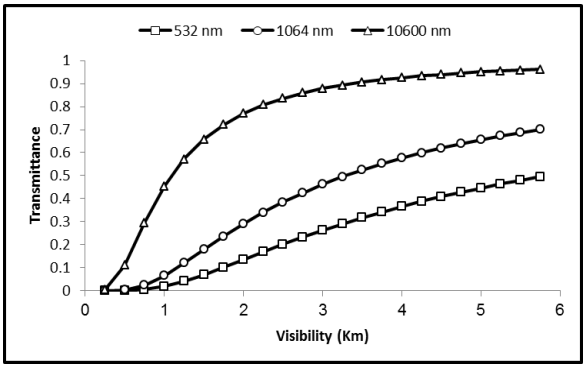

Figure 3. Atmospheric transmittance of wavelength (532, 1064, and 10600) nm dependent on visibility distance for bad weather.

4.2. Calculation of the beam attenuation due to dust in Hilla city

Figure (4) which represent variations of transmittance as a function of dust concentration with propagation distance of 10 km for a dust concentration (C=95.59 $\mu g / m^3$) and for the three wavelengths its shows that the wavelength of 10600 nm is capable to penetrate dust effect in the path length than the other two wavelengths (532, 1064 nm), and wavelength of 1064 nm has better capablty to overcome effect of dust than the wavelength of 532 nm.

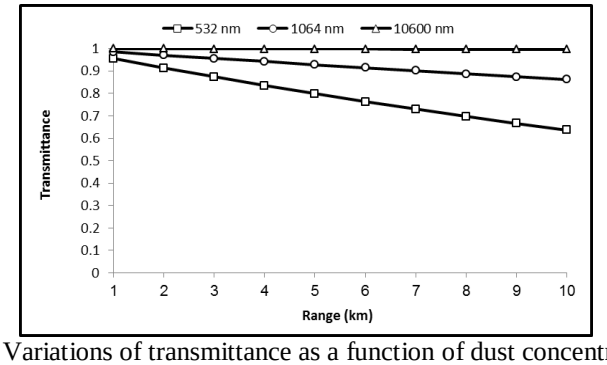

Figure 4. Variations of transmittance as a function of dust concentration, for (C= 95.59 $\mu g / m^3$) for the three wavelengths, for path length of 10 km.

Figure (5) represent variations of transmittance as a function of dust concentration with propagation distance of 10 km, concentration of dust (C= 343.71 $\mu g / m^3$), we saw twice time that wavelength of 10600 nm has high capability to overcome dust effect, the transmittance of 10600 nm at 10 km distance approach to 0.99 value, while the value of transmittance of wavelength 1064 nm approach to 0.81 value, and 532 nm approach to 0.55 at distance of 10 km.

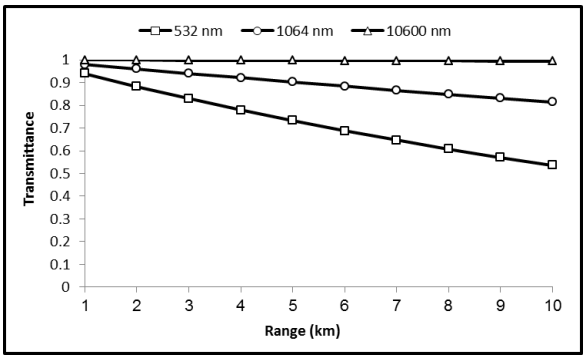

Figure 5. Variations of transmittance as a function of dust concentration, for (C= 343.71 $\mu g / m^3$), for the three wavelengths, for path length of 10 km.

Figure (6) represents variations of transmittance as a function of dust concentration with propagation distance of 10 km, concentration of dust (C= 450.95 $\mu g / m^3$), we saw that the transmittance of wavelength 10600 nm value of 0.99, while wavelengths of (1064, and 532) nm, values of (0.77 - 0.47) respectively at distance propagation of 10 km.

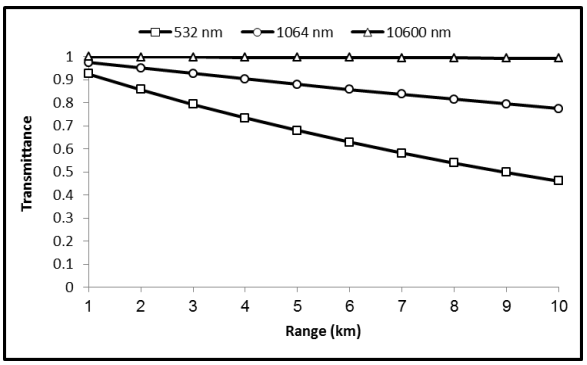

Figure 6. Variations of transmittance as a function of dust concentration, for (C= 450.95 $\mu g / m^3$), for the three wavelengths, for path length of 10 km.

Figure (7) represent variations of transmittance as a function of dust concentration with propagation distance of 10 km, concentration of dust (C= 50.762 $\mu g / m^3$), we saw that the transmittance of wavelength 10600 nm value more than 0.99 at distance of 10 km, while wavelengths 1064 nm, and 532 nm have transmittance of 0.96, and 0.88 respectively at propagation distance of 10 km, which lead to more capability of wavelength 10600 nm than the wavelengths of 1064 nm, and 532 nm of penetrating effects of dust.

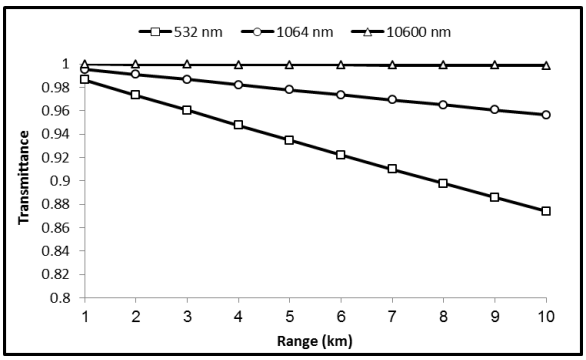

Figure 7. Variations of transmittance as a function of dust concentration, for (C= 50.762 $\mu g / m^3$), for the three wavelengths, for path length of 10 km.

Figure (8) represents variations of transmittance as a function of dust concentration with propagation distance of 10 km, concentration of dust (C= 707.79 $\mu g / m^3$), we saw that the transmittance of wavelength 10600 nm value of 0.99, while wavelengths of (1064, and 532) nm, values of (0.7 - 0.37) respectively at distance propagation of 10 km.

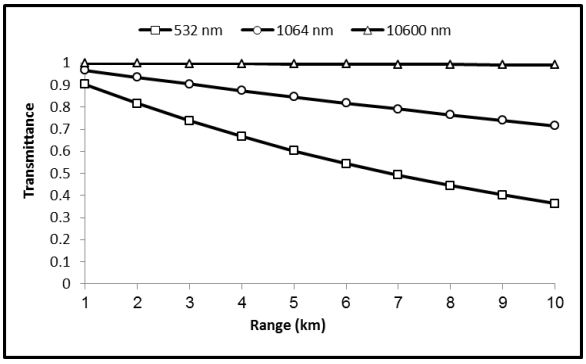

Figure 8. Variations of transmittance as a function of dust concentration, for (C= 707.79 $\mu g / m^3$), for the three wavelengths, for path length of 10 km.

Figure (9) represent variations of transmittance as a function of dust concentration with propagation distance of 10 km, concentration of dust (C= 937.05 $\mu g / m^3$), we saw wavelength of 10600 nm has high capability to overcome dust effect, the transmittance of 10600 nm at 10 km distance approach to 0.98 value, while the value of transmittance of wavelength 1064 nm approach to 0.55 value, and 532 nm approach to 0.22 at distance of 10 km.

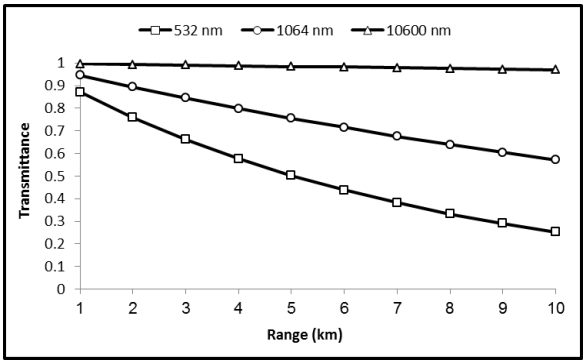

Figure 9. Variations of transmittance as a function of dust concentration, for (C= 937.05 $\mu g / m^3$), for the three wavelengths, for path length of 10 km.

From the figures, we saw that the wavelength of 10600 nm has more operative than wavelengths of 1064 nm, and 532 nm to overcome the effect of dust because their higher wavelength comparing with other wavelength.

5. CONCLUSIONS

1. In Iraq the effect of dust is approximately high effect because of there climate area in Iraq are semi desert area (desert climate).
2. Laser beam of wavelength (10600 nm) is more practical in laser communication than both the 532&1064 nm.
3. The best use of laser beam propagation is through clear weather especially in winter period, because of the decrease in temperature and the absence of any turbid phenomenon which reduces the visibility range to less than 10 km. scattering of laser beam is at most constant in clear weather.

REFERENCES

[1] L. C. Andrews, "Free-Space Laser Propagation: Atmospheric Effects", IEEE Journal, Vol. 19, No. 5, P.6-8, October (2005).
[2] O. Bouchet and H. Sizun ,"Free-Space Optics Propagation and Communication", ISTE Ltd, USA, (2006).
[3] V. W. Chan, "Free-Space Optical Communications", Journal of Lightwave Technology, Vol. 24, No. 12, P.4750-4762, December (2006).
[4] H. Hemmati, "Deep Space Optical Communications", NASA, California Institute of Technology, USA, October (2005).
[5] I. Kim, B. Arthur, and E. Korevaar, "Comparison of laser beam propagation at 785 nm and 1550 nm in fog and haze for optical wireless communications", Optical Wireless Communication III, Proc. SPIE, 4214, (2001).
[6] A. Komaee, P. S. Krishna, and P. Narayan, "Active Pointing Control for Short Range Free-Space Optical Communication", Communications in Information and Systems Journal, Vol.7, No. 2, P. 177-194, (2007).
[7] E. Korevaar, I. Kim, and B. Arthur, "Debunking the recurring myth of a magic wavelength for free-space optics", SPIE Journal, Vol. 4873, P.155-161, (2002).
[8] E. Kozachenko and M. Anderson, "A Free Space Optical Communications System", IEEE Journal, Vol. 1, No. 3, P. 195- 201, (2011).

METHODS AND ALGORITHMS FOR GENERATION OF RANDOM LOW FREQUENCY SERIES OF SIGNALS FOR MAGNETOTHERAPY

A. D. Dimitrov*, K. L. Dimitrov**

*Technical University of Sofia, Bulgaria, Faculty of Telecommunication, TU-Sofia,
"Kl.Ohridsky" str. 8, 1000 Sofia, Bulgaria,
e-mail: atanas.dimitrov@best.eu.org
**Technical University of Sofia, Bulgaria, Faculty of Telecommunication, TU-Sofia,
"Kl.Ohridsky" str. 8, 1000 Sofia, Bulgaria,
e-mail:kld@tu-sofia.bg

Abstract

Today most of the medical systems for magneto therapy contain digital control unit which provides more advanced features for treatment of different diseases. New systems for magneto therapy with pseudo-random frequency hopping provide more opportunities and better medical results.

The method described in this article shows new innovative way of generation of pseudo-random low frequency magnetic field. Due to the randomness character of device's output signals would be achieved reduced adaptation by human body to the influence of magnetic field and better treatment of different diseases.

However this algorithm is more complex it does not requires usage of any additional elements and investment of high costs. The application of software methods for generation of pseudo-random signal frequency hopping in systems for magneto therapy can open new possibilities for treatment of more health diseases with better clinical results.

1. INTRODUCTION

Usually every system for physiotherapy contains microcontroller with appropriate uploaded firmware. This is also the main unit for digital control of system for magneto-therapy with pseudo-random low frequency magnetic field. The main component of the systems for magneto therapy using low frequency magnetic field is digital controlled generator for rectangular electrical impulses with special parameters. Programmable logic of one-chip generators is a great advantage over the basic generators. Any functional change can be implemented easily without any hardware changes.

2. BLOCK DIAGRAM OF THE SYSTEM FOR MAGNETO THERAPY BY RANDOM LOW FREQUENCY SERIES OF SIGNALS

The block diagram of above mentioned system for magneto therapy can be seen on Figure 1. There are seven functional blocks. Working modes of therapy system can be described as follows:

The output of the Main control unit generates series of rectangular digital impulses to the Unit for commutation of the output signals. Amplitude of the output signals of the systems is determined by the Unit for amplitude control. External user control of the working frequency is possible thanks to Unit for external frequency control. There are also liquid crystal displays for visualization of the parameters of output pulses for the system in real time.

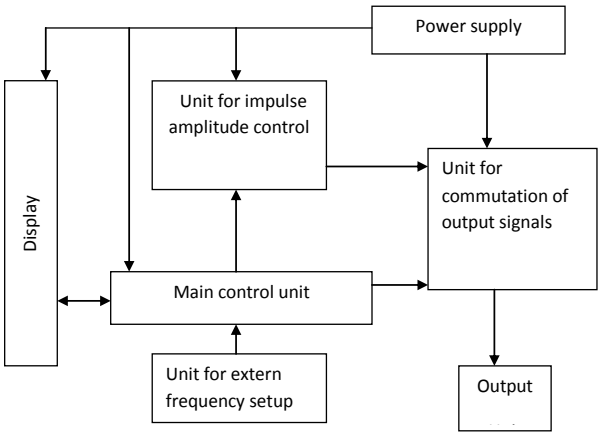

Figure1. Block-diagram of systems for magneto therapy with "running" magnetic field

The Main control unit is the most important part of the system and it has to and control the working modes and to analyze signals form the "*Unit for amplitude control block*", "*Unit for commutation output signals*", "*Unit for extern frequency setup*".

This block is responsible for: the time for generating periodic pulses, the maximum operating frequency, amplitude and duty cycle of the system output signals. The change the operating mode of this module is possible by detecting the signals coming from "Unit for external frequency setup".

Main task of control unit of the device is to process all external user requests and generate appropriate low frequency random signal depending selected settings by the user. In addition control unit has to manage the actions of all other related functional system's blocks:

- External control unit;

- Output signal commutation;
- Amplitude control unit;
- Signal processing unit

It is necessary to be provided software user interaction for system's management. Because of that the main function of pre-uploaded internal program of microcontroller firmware has to contain endless loop. System initialization process includes primary configuration of all functional microcontrollers' peripheral blocks and loading of initial values for all software variables. Primary initialization of the controller is invoked each time when the system is powered on. For appropriate device's operation all Input/ Output ports of the microcontroller must be configured in accordance with the principle scheme of the system. To enable external user control of the system are could be used four tact-buttons, which have to be connected to input pins of the microprocessor. The providing of this type of user control requires constant monitoring of button status. For reducing of noise signals or wrong signals from the buttons there

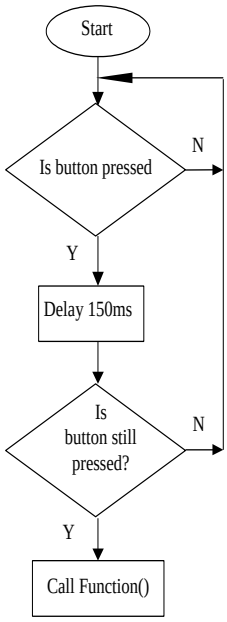

Figure 2. Algorithm for registering of input signals from external buttons

is checking function which checks: "is there any continuously pressed button". One algorithm for implementation of this functional can be seen on Figure 2.

If there is a pressed button after defined time delay of 150ms, the same button is checked again. In case when the button is pressed for longer time than defined time delay, controllers recognize input signal as real and call defined software function.

On each cycle of the main subprogram the four input pins of the microprocessor are checked. Logic program can be divided into five main units. External control unit consists of four push buttons submitting input to four input terminals defined by the microprocessor. Each button is configured to call different function in execution of the main program. By pressing button "electrical signal" a logical "0" will be sent to the processor's inputs. The Unit for commutation of the output consists five output drivers, which are connected to the microprocessor's output pins. Amplitude control unit consist six outputs. They are used for determination of the amplitudes of output signals. Signal processing unit consists of microcontroller with appropriate uploaded firmware on it. As signal pulse generation an internal timer block is used. Each timer's overflow can cause interrupt of the main program and can call function for signal's level change. The pseudo-random frequency hopping is implemented thanks additional software random function.

3. PSEUDO - RANDOM SIGNAL GENERATION

Pseudo-random numbers are generated by software functions. They are referred to as "pseudo-random" because the sequence of numbers is determined preliminary. Given a particular function and a "seed" value, the same sequence of numbers will be generated by the function. If the pseudo-random number generation function is well designed, the sequence of numbers will appear to be statistically random. The pseudo-random number generation functions available in most standard computer math

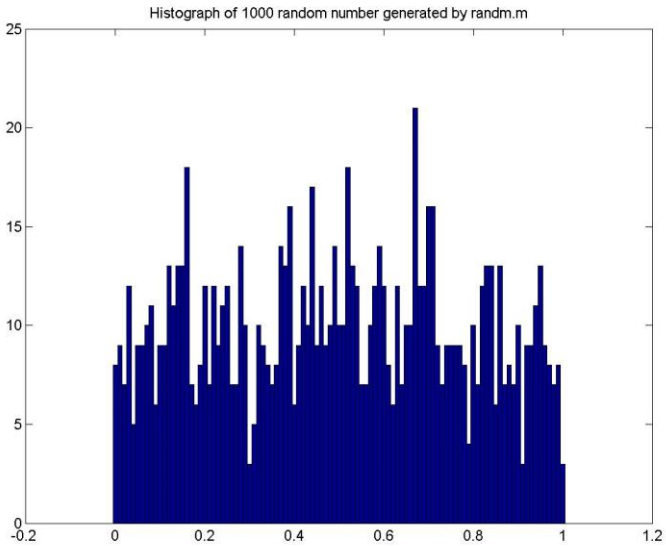

Figure 3. Histogram of 1000 random values generated by software random function

libraries generate random numbers with a uniform distribution. If many "random" numbers are drawn from a particular region, where the value **v** is in the range 0 <= v < 1) and a Histogram plot is generated from the result, the histogram will form a block. The pseudo-random number generation functions available in most standard computer math libraries generate random numbers with a uniform distribution. If many "random" numbers are drawn from a particular region, where the value, **v** would be in the range 0 <= v < 1) and a histogram plot is generated from the result (Figure 3).

A Linear Congruential Generator (LCG) represents one of the best-known pseudorandom number generator algorithms, which is easily implemented and fast.

The generator is defined by the recurrence relation:

$$X_{n+1} \equiv (aX_n + c) \pmod{m} \tag{1}$$

,where X_n is the sequence of pseudorandom values, and :

$m,\ 0 < m$ — the "modulus"

$a,\ 0 < a < m$— the "multiplier"

$c,\ 0 \leq c < m$— the "increment"

$X_0,\ 0 \leq X_0 < m$ — the "seed" or "start value" are integer constants that specify the generator.

If c = 0, the generator is often called a multiplicative congruential method, or Lehmer RNG. If c ≠ 0, the generator is called a mixed congruential method [2].

The Period → The period is the smallest positive integer λ for which $X_\lambda = X_0$. The period can be no greater than m. Therefore, m is chosen to be equal or nearly equal to the largest representable integer in the computer to get a long period.

A full period generator is one in which the period is m, and it is obtained:

- c is relatively prime to m;

- (a-1) is a multiple of q, for each prime factor q of m;

- (a-1) is a multiple of 4,

The Increment - If c > 0, we can achieve a full period by such:

- m =2^b → faster computer arithmetic,

- Set (a-1) as a multiple of 4,

- c should be odd-valued,

- Set b as high as possible. For example b=31 in a 32-bit computer.

If c = 0, a full period is not possible.

Then a maximum number of random variables can be achieved.

A maximum period generator, with $\lambda = m - 1$, is one in which a is a primitive element modulo m, if m is prime.

4. ALGORITHMS FOR AUTOMATIC GENERATION OF PSEUDO-RANDOM SIGNALS

The microprocessor work in endless loop that consistently reviewed and adjusted with predefined parameters of the generated signals and modes of the generator. The procedure for generating pulses continues until the time specified by the user expired or if external button is pressed. Algorithm of work on the main subprogram is shown on Figure 4. When the system is powered on first are invoked functions for primary initialisation of microcontroller's configuration registers. After all of registers are set with appropriate values is called initialisation function and primary values for working variables are loaded. If button "Set" is pressed by the user the parameters of output signal could be checked or modified. Execution of the main function for signal generations starts when button Start is pressed. The series of signals are generated automatically till predefined period of time is expired or till button Stop is pressed. External interaction by the user during the active process of the function is also possible. User is able to increase/decrease in real-time the frequency of the output signal with buttons Up or Down. In this case the function for automatic frequency hopping will be disabled and system will work in manual mode. By pressing button Start button again will reactivate automatic mode of the system. In case Stop button is pressed one time system will halt generation process. If Stop button is pressed one more time the main function will be stopped, otherwise if start button is pressed the series of signals will be generated till predefined time expires.

The signal amplitude can be changed automatically during the process of therapy or to be fixed precisely. To achieve feedback from the user and easy monitoring of the operating mode of the microprocessor function is done using an infinite loop. Therefore

the microprocessor always waits intervention by the user before an operation. In primary set automatic mode switching for the amplitude of the output signals of each

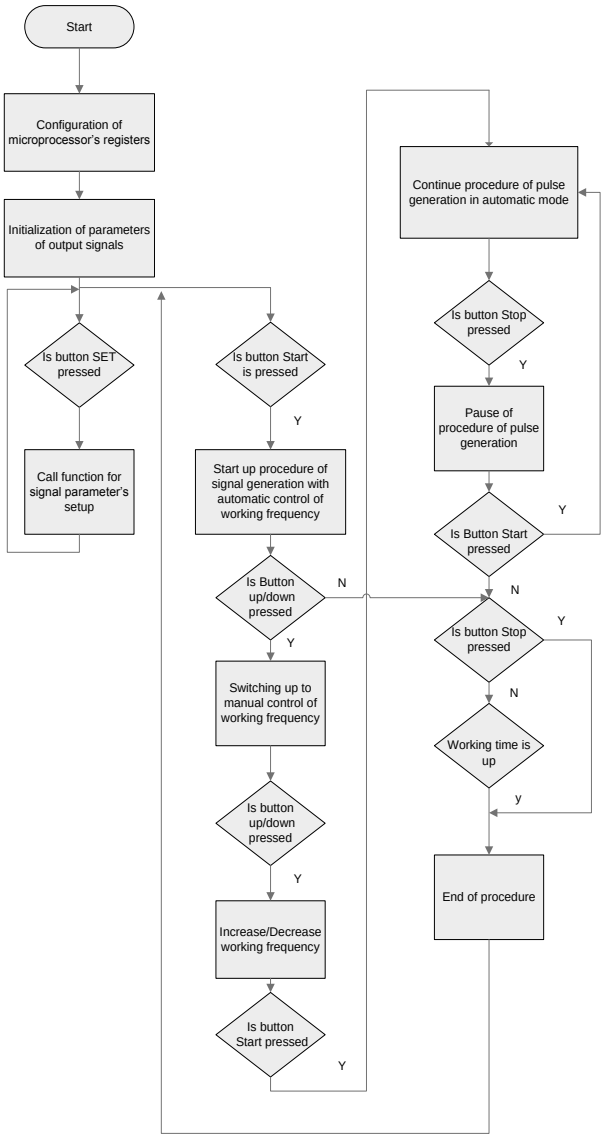

Figure 4. Algorithm of work on the main subprogram

device to switch from maximum to minimum frequency is automatically switched the amplitude of the output.

Random switching of amplitude as a function of time can be seen on Fig. 5. The time remaining until the end of the procedure is kept in memory of the processor and then return back in the automatic mode continues to check the time remaining. In manual mode the user can increase the frequency of pulses generated by pressing Up, a Down

button to reduce it. Switching back in the automatic mode is performed after pressing Start.

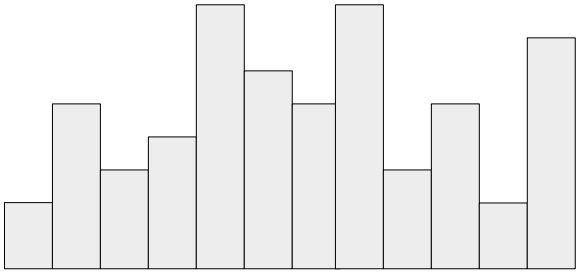

Figure 5. Switching amplitude as a function of time

After initialization process starts the process of generating pulses from the microprocessor. When the highest frequency is reached, it is automatically switches back to the lowest. Any such transition is related to increased unit with a variable voltage to determine what is fed to the outputs of the device. After reaching the maximum frequency used for all terminals controlling the output voltage is reset. Termination of the procedure for generating pulses occurs when it detects a double interference by the user or if the time set for the procedure of generations has elapsed. CPU returns to waiting mode output, which monitors the re-intervention by the user. The process of generation of pulse sequences with automatic changing of frequency is shown Figure 6.

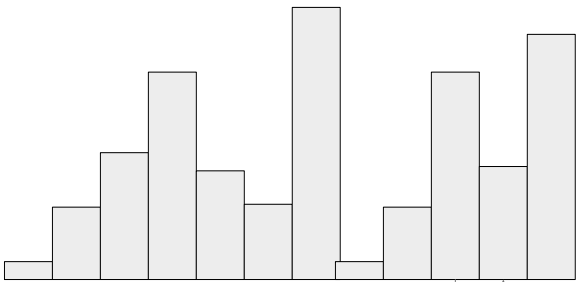

Figure 6. Generation process of pseudo-random pulse sequences with automatic frequency changing

On Figure 7 can be seen algorithm of the process of generating a certain periodical series of rectangular pulses with automatically change of amplitude and frequency. The structure and explanation of this algorithm is described below.

Before the beginning of the procedures for pulse generation all software variables are initialized with appropriate values. Internal for the controller Timer block, responsible for pulse's period is also set. After initialization process is completed and internal timer is activated the signal's generation process can be started. There is external source for signal generation with frequency of 1Hz. Each program interrupt from the

external source will cause interrupt of the process and will increment counting variable. Every fifth interrupt will cause automatically switch to next higher signal's

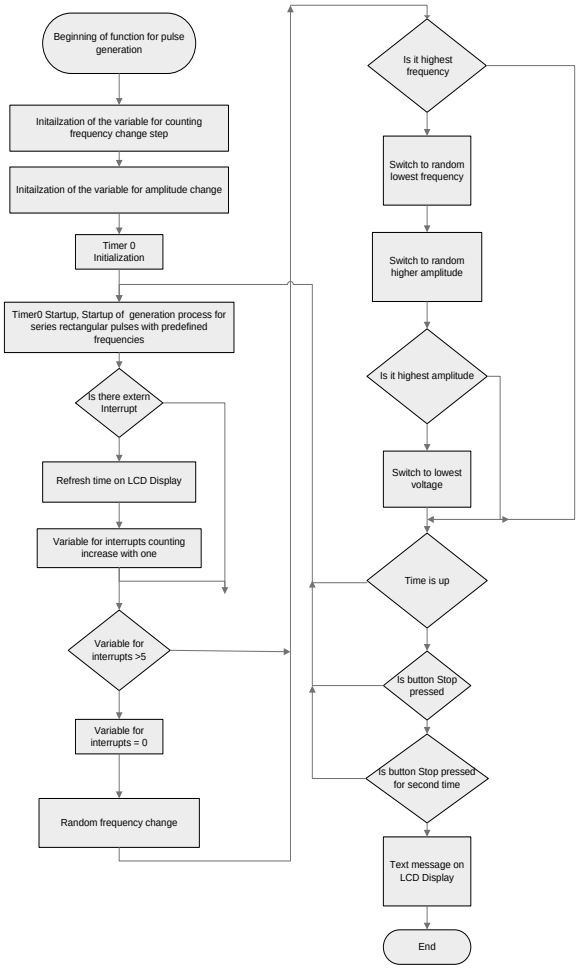

Figure 7. Algorithm of process of generating a certain random series of rectangular impulses

frequency with random step. If the next higher frequency is above defined by the user frequency's maximum system will switch to lowest randomly selected frequency value, which is close to defined frequency minimum. Each switch from maximum to minimum will cause also automatically increase of signal's amplitude with random step also. When next amplitude's value is higher than defined maximum the system will switch automatically to another random selected lower value. All described processes will repeat till the program is stopped from the user by pressing of 'Stop' button or until defined time is expired.

3. CONCLUSION

New algorithms for management and control of system for therapy by magnetic field with random low frequency hopping are presented in the paper. These

algorithms provided a high level of flexibility not only for above mentioned system for magneto therapy, but for other different microprocessor systems for physiotherapy. The presented algorithms provide very friendly changing of different modes of therapy. In the same time the system can provide many modes of therapy. Some of them can be very complicated. The number of modes of therapy provided by this kind of algorithms is not limited. The assurance of described system, which is provided by algorithms for CPU is an other very important advantage.

REFERENCES

[1] SIEMENS Medical Engineering Group, "Units for Physical Therapy And Diagnosis", p.230, 2002

[2] W. Y. Riadh, "Electromagnetic Fields and Radiation (Human Bioeffects and Safety)", Marcel Dekker Inc. Canada, 2001,ISBN 0-8247-0877-3.

[3] V. Mihaylov, Kalin L. Dimitrov, Dimitar C. Dimitrov, Research on the influence of permanent magnetic field during live tissue laser treatment, 3rd International Conference "Communication, Electromagnetism and Medical Application, Athens, Greece, November 6-8, 2008, p.12-156.

[4] Gentle, James E., (2003). Random Number Generation and Monte Carlo Methods, 2nd edition, Springer, ISBN 0-387-00178-6.

[5] http://www.bearcave.com/misl/misl_tech/wavelets/hurst/random.html

[6] http://rosettacode.org/wiki/Linear_congruential_generator#

[7] http://www.public.iastate.edu/~riczw/stat330s11/supp/rng_330_1.pdf

[8] http://www.math.ucsd.edu/~maebrahi/SDE/random.htm